

Stabilization of CO₂ as Zwitterionic Carbamate within a Coordination Polymer (CP): Synthesis, Structure and Anions Sensing Behaviour of Tb-CP composite

Sourav Sarkar,^a Debal Kanti Singha,^{a,b} Prakash Majee,^b Pooja Daga,^b Sudip Kumar Mondal^{b*}
and Partha Mahata^{a*}

^aDepartment of Chemistry, Jadavpur University, Kolkata-700032, India. Email: parthachem@gmail.com

^bDepartment of Chemistry, Siksha-Bhavana, Visva-Bharati University, Santiniketan-731235, West Bengal, India. Email: sudip.mondal@visva-bharati.ac.in

ELECTRONIC SUPPLEMENTARY INFORMATION

Table S1: Selected bond angles observed in $[\text{Gd}(3,5\text{-pydc})_{1.5}(\text{CO}_2)_{0.5}(\text{H}_2\text{O})_4].3\text{H}_2\text{O}$, **1**.

Angle	Amplitude ($^{\circ}$)	Angle	Amplitude ($^{\circ}$)
O(5)-Gd(1)-O(9)	71.91(13)	O(5)-Gd(1)-O(8)	127.16(14)
O(5)-Gd(1)-O(10)	135.42(12)	O(9)-Gd(1)-O(8)	73.32(15)
O(9)-Gd(1)-O(10)	78.61(13)	O(10)-Gd(1)-O(8)	71.91(13)
O(5)-Gd(1)-O(11)	144.03(13)	O(11)-Gd(1)-O(8)	72.02(15)
O(9)-Gd(1)-O(11)	141.96(13)	O(1)-Gd(1)-O(8)	143.62(14)
O(10)-Gd(1)-O(11)	76.19(13)	O(5)-Gd(1)-O(3)#1	75.68(13)
O(5)-Gd(1)-O(1)	89.19(13)	O(9)-Gd(1)-O(3)#1	98.04(12)
O(9)-Gd(1)-O(1)	127.62(13)	O(10)-Gd(1)-O(3)#1	142.31(12)
O(10)-Gd(1)-O(1)	83.00(12)	O(11)-Gd(1)-O(3)#1	85.29(14)
O(11)-Gd(1)-O(1)	76.77(13)	O(1)-Gd(1)-O(3)#1	124.55(11)
O(8)-Gd(1)-O(3)#1	71.23(13)	O(5)-Gd(1)-O(4)#1	73.11(12)
O(9)-Gd(1)-O(4)#1	138.59(12)	O(10)-Gd(1)-O(4)#1	142.80(12)
O(11)-Gd(1)-O(4)#1	71.13(12)	O(1)-Gd(1)-O(4)#1	72.76(11)
O(8)-Gd(1)-O(4)#1	112.90(13)	O(3)#1-Gd(1)-O(4)#1	51.79(10)
O(5)-Gd(1)-O(2)	71.73(12)	O(9)-Gd(1)-O(2)	76.14(12)
O(10)-Gd(1)-O(2)	69.20(11)	O(11)-Gd(1)-O(2)	119.42(13)
O(1)-Gd(1)-O(2)	51.48(11)	O(8)-Gd(1)-O(2)	134.21(13)
O(3)#1-Gd(1)-O(2)	147.10(12)	O(4)#1-Gd(1)-O(2)	112.63(10)

Symmetry transformations used to generate equivalent atoms: #1 x,-y+1,z-1/2

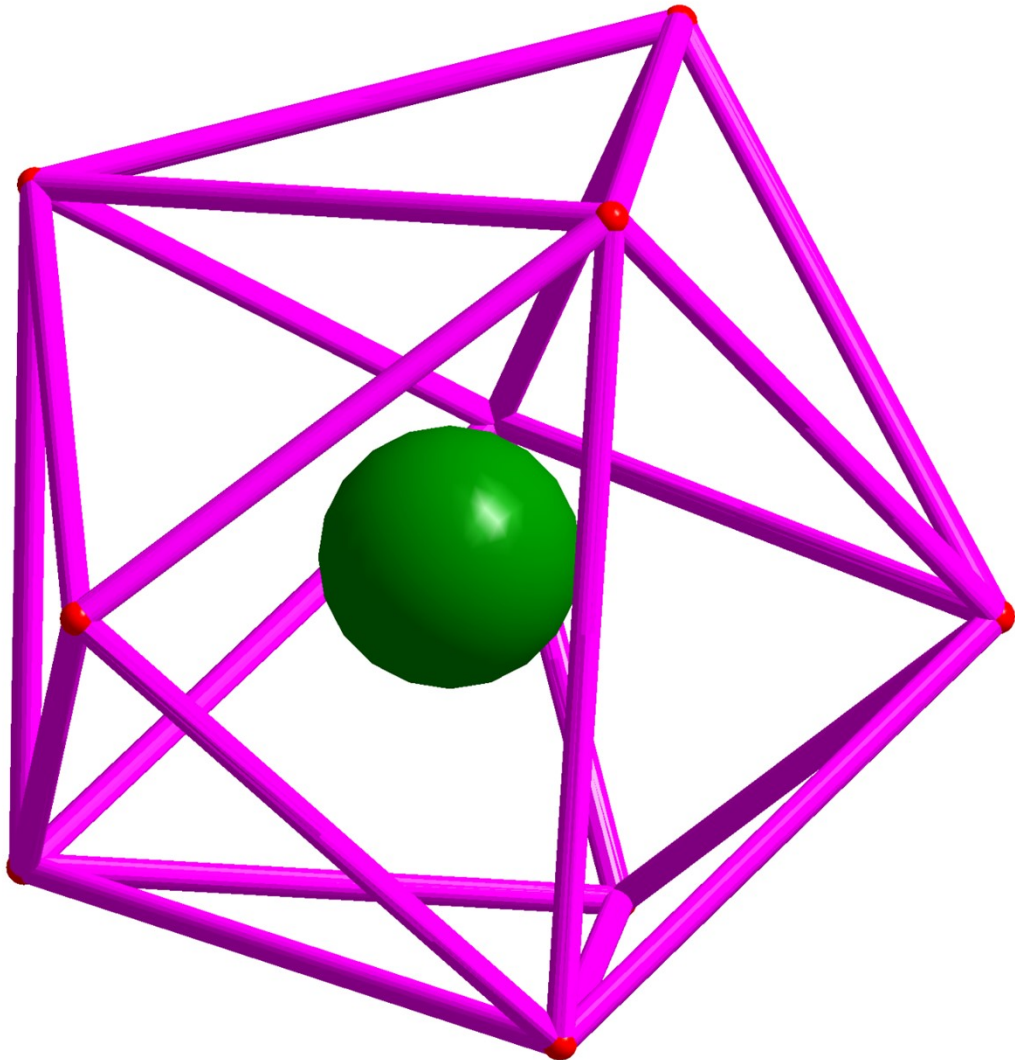


Fig. S1. Figure shows nine coordinated polyhedral unit $[\text{GdO}_9]$ with distorted tricapped trigonal prismatic geometry in $[\text{Gd}(3,5\text{-pydc})_{1.5}(\text{CO}_2)_{0.5}(\text{H}_2\text{O})_4]\cdot 3\text{H}_2\text{O}$, **1**.

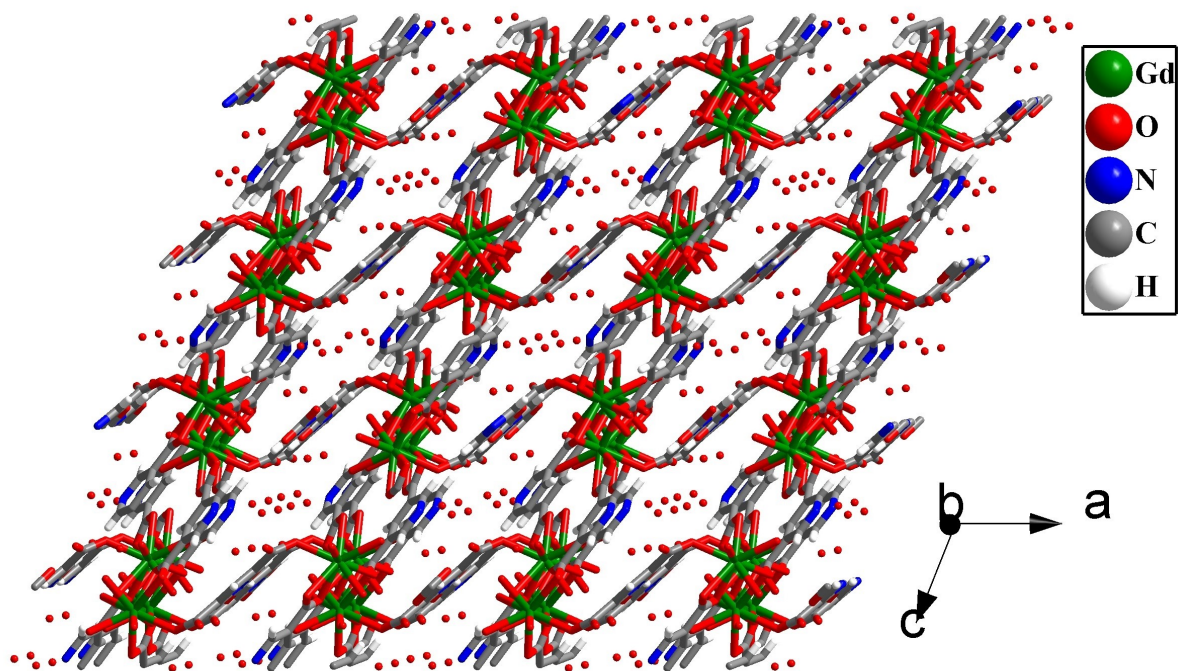


Fig. S2. Figure shows three-dimensional supra-molecular structure stabilized through hydrogen bond interactions involving coordinated water molecules in $[\text{Gd}(\text{3,5-pydc})_{1.5}(\text{CO}_2)_{0.5}(\text{H}_2\text{O})_4].3\text{H}_2\text{O}$, **1**.

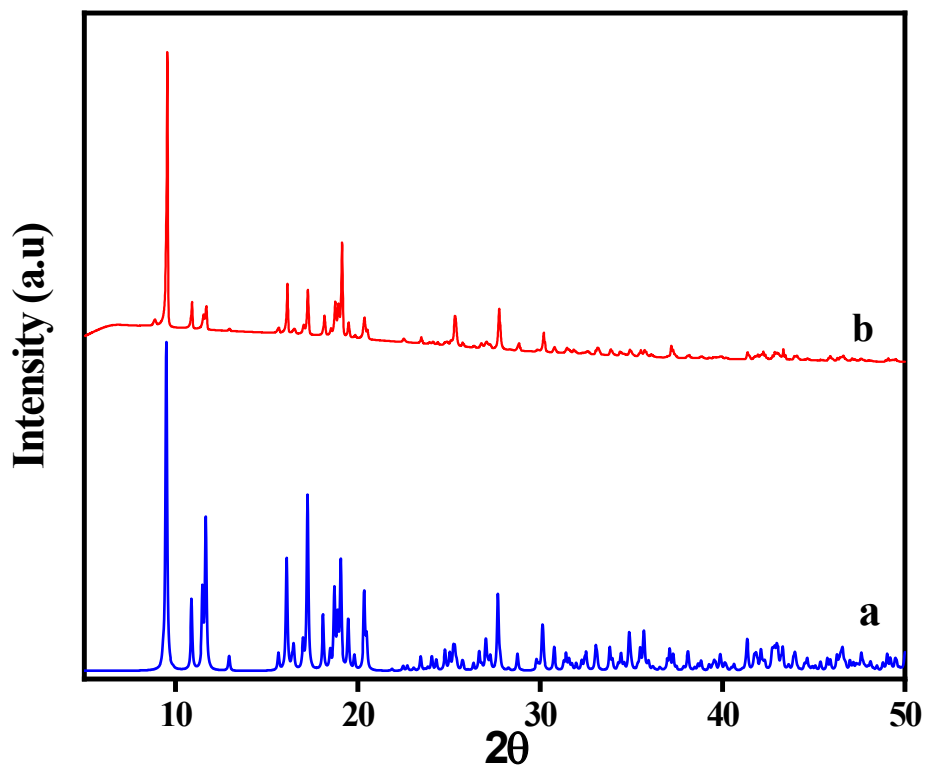


Fig. S3. Powder XRD (CuK α) patterns of (a) simulated from single crystal X-ray data (b) experimental of [Gd(3,5-pydc)_{1.5}(CO₂)_{0.5}(H₂O)₄]₃H₂O, **1**.

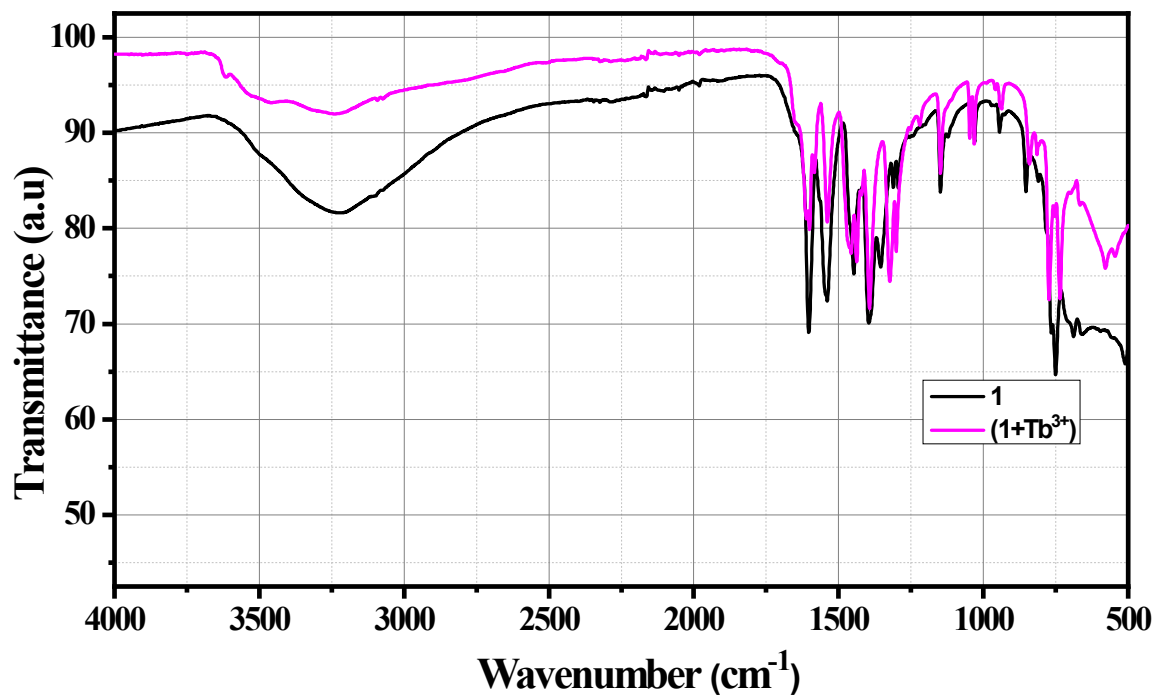


Fig. S4. FTIR spectra of compound **1** and **1+Tb³⁺** (Tb@**1**).

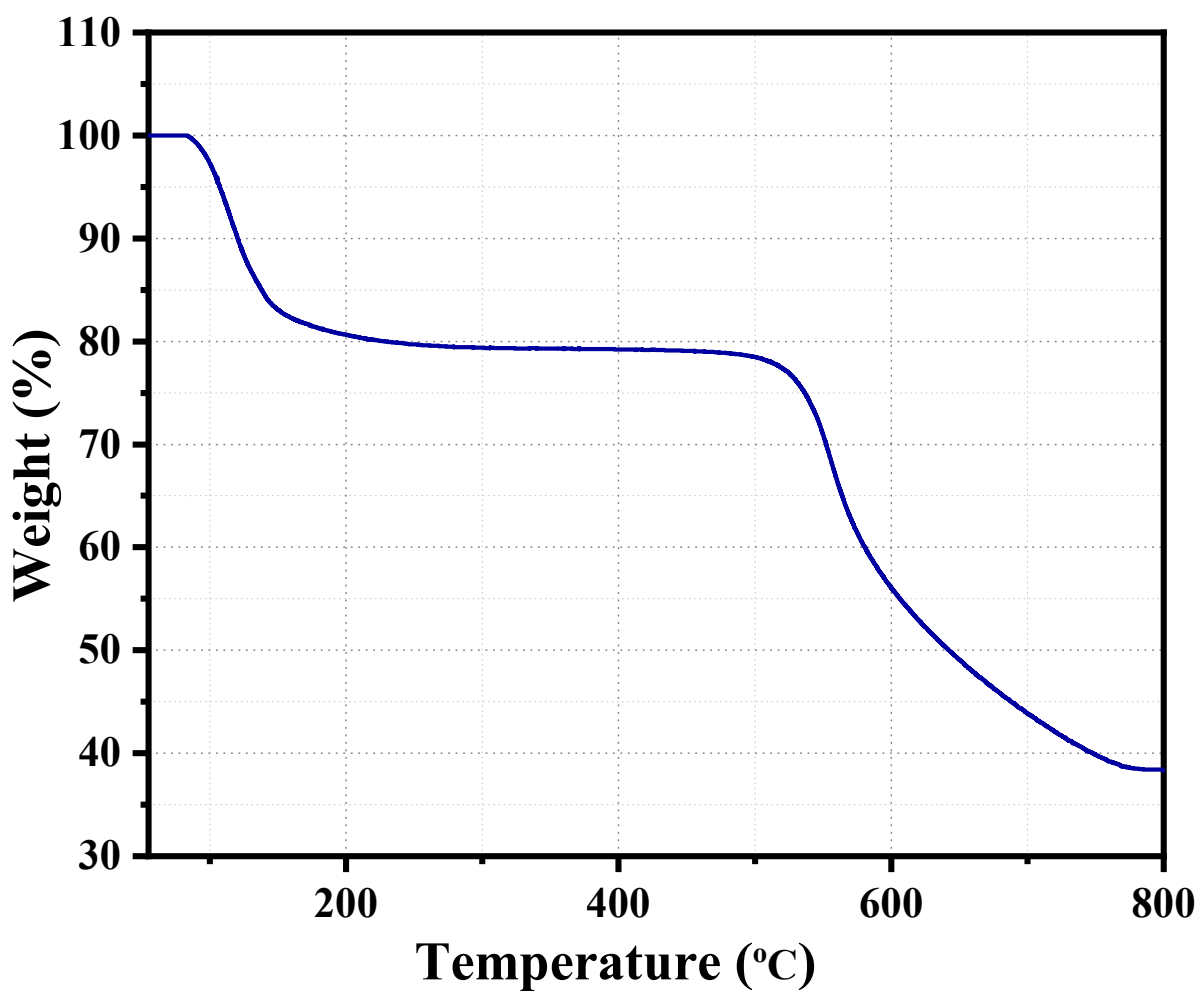


Fig. S5. Thermogravimetric analysis (TGA) of $[\text{Gd}(3,5\text{-pydc})_{1.5}(\text{CO}_2)_{0.5}(\text{H}_2\text{O})_4].3\text{H}_2\text{O}$, **1**, in nitrogen atmosphere.

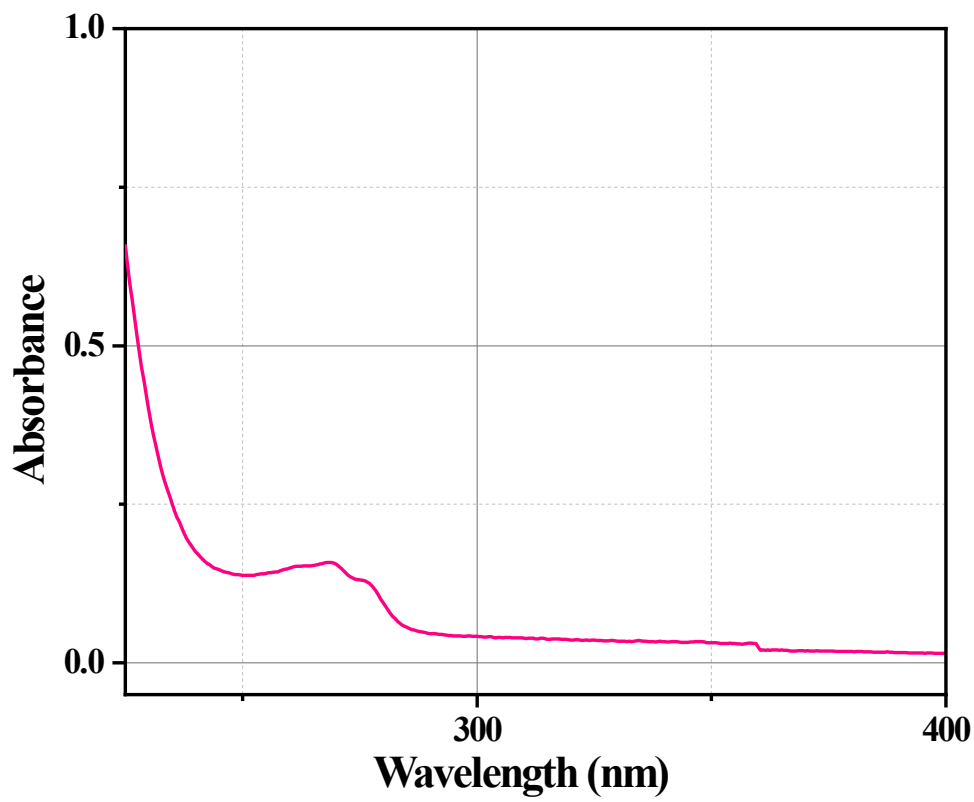


Fig. S6. Figure shows absorption spectrum of $[\text{Gd}(3,5\text{-pydc})_{1.5}(\text{CO}_2)_{0.5}(\text{H}_2\text{O})_4]\cdot 3\text{H}_2\text{O}$, **1**, dispersed in water.

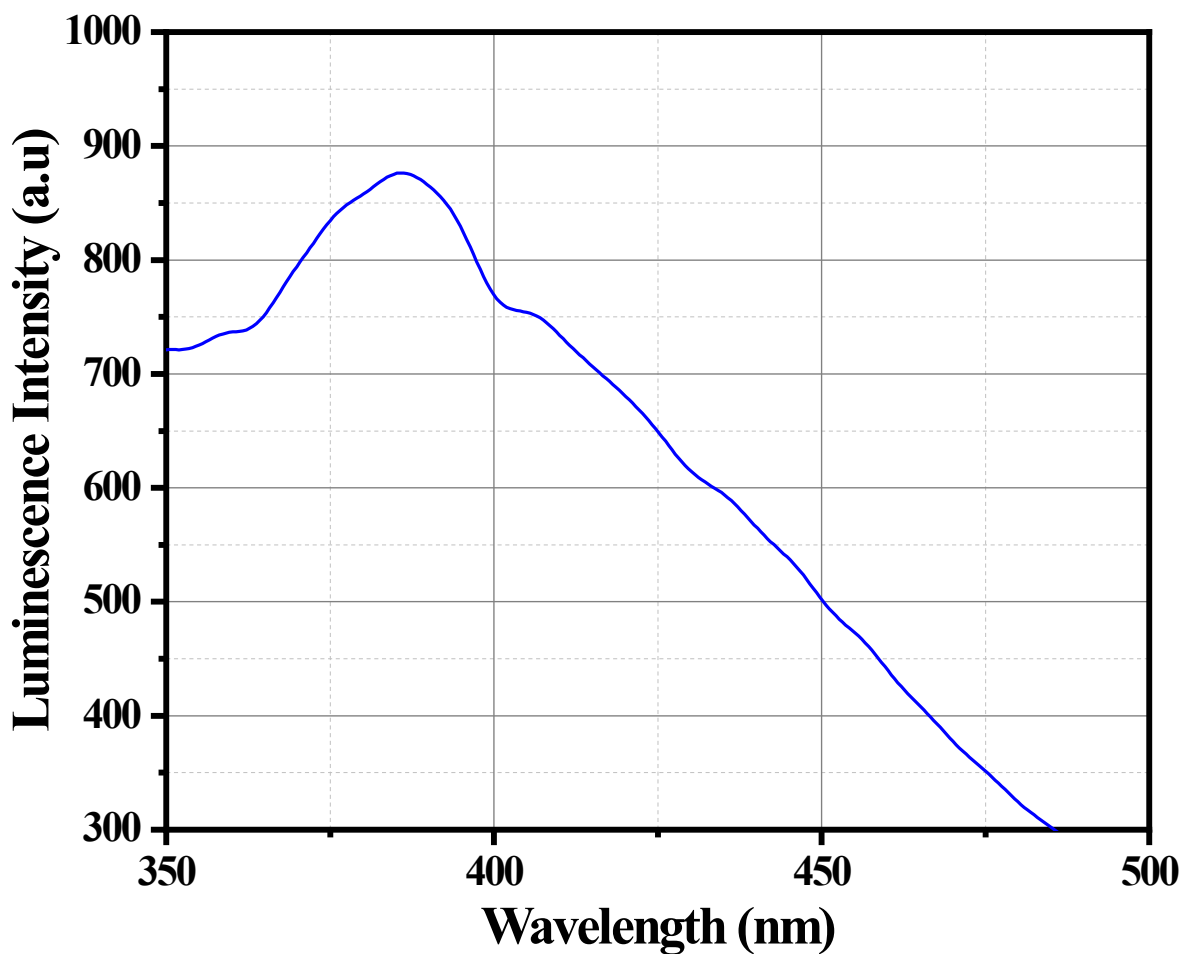


Fig. S7. Emission spectrum of $[\text{Gd}(3,5\text{-pydc})_{1.5}(\text{CO}_2)_{0.5}(\text{H}_2\text{O})_4].3\text{H}_2\text{O}$, **1**, dispersed in water upon excitation at 270 nm.

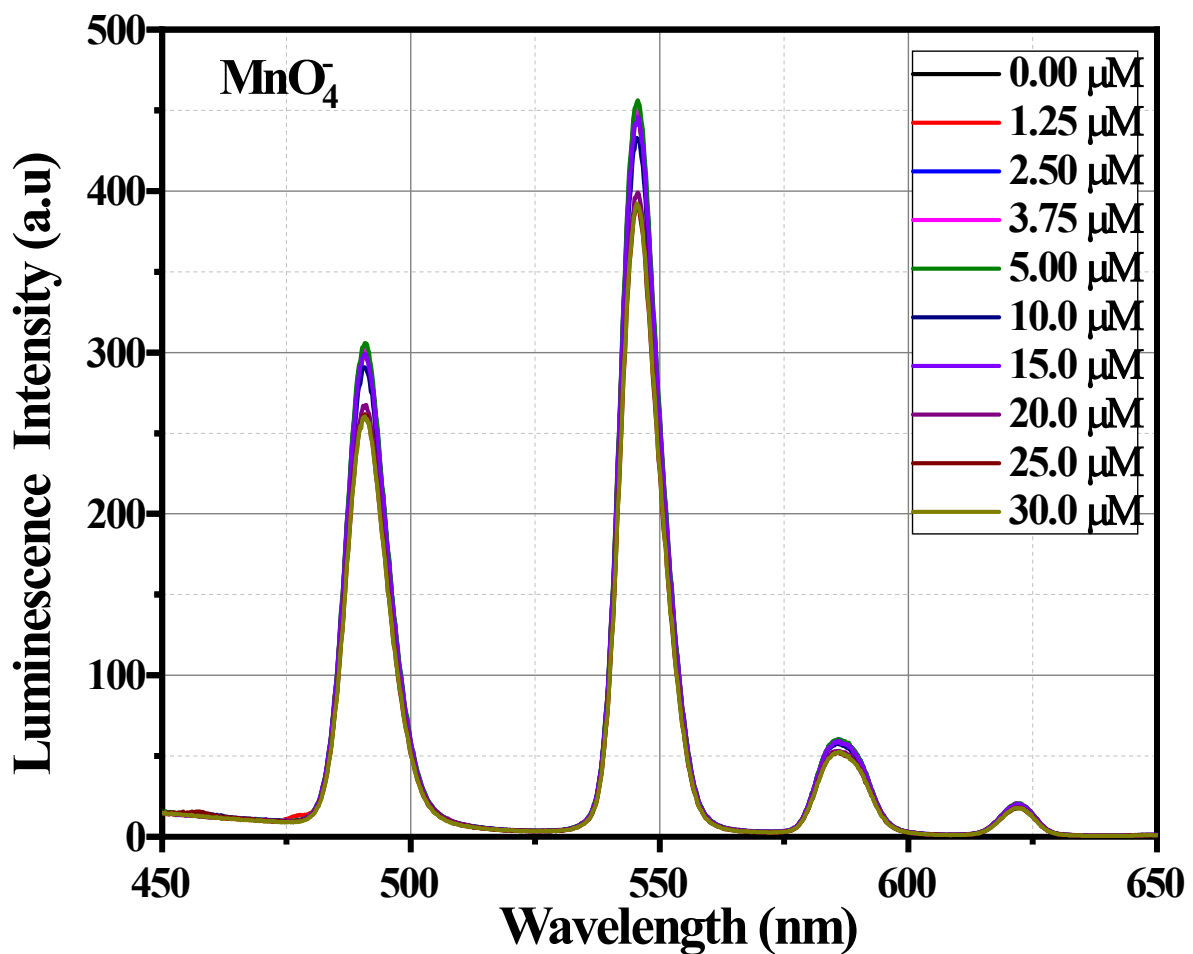


Fig. S8. Emission spectra of **Tb@1** dispersed in water upon the incremental addition of an aqueous solution of MnO_4^- ions ($\lambda_{\text{ex}} = 270 \text{ nm}$). The final concentration of MnO_4^- ions in the medium is indicated in the legend.

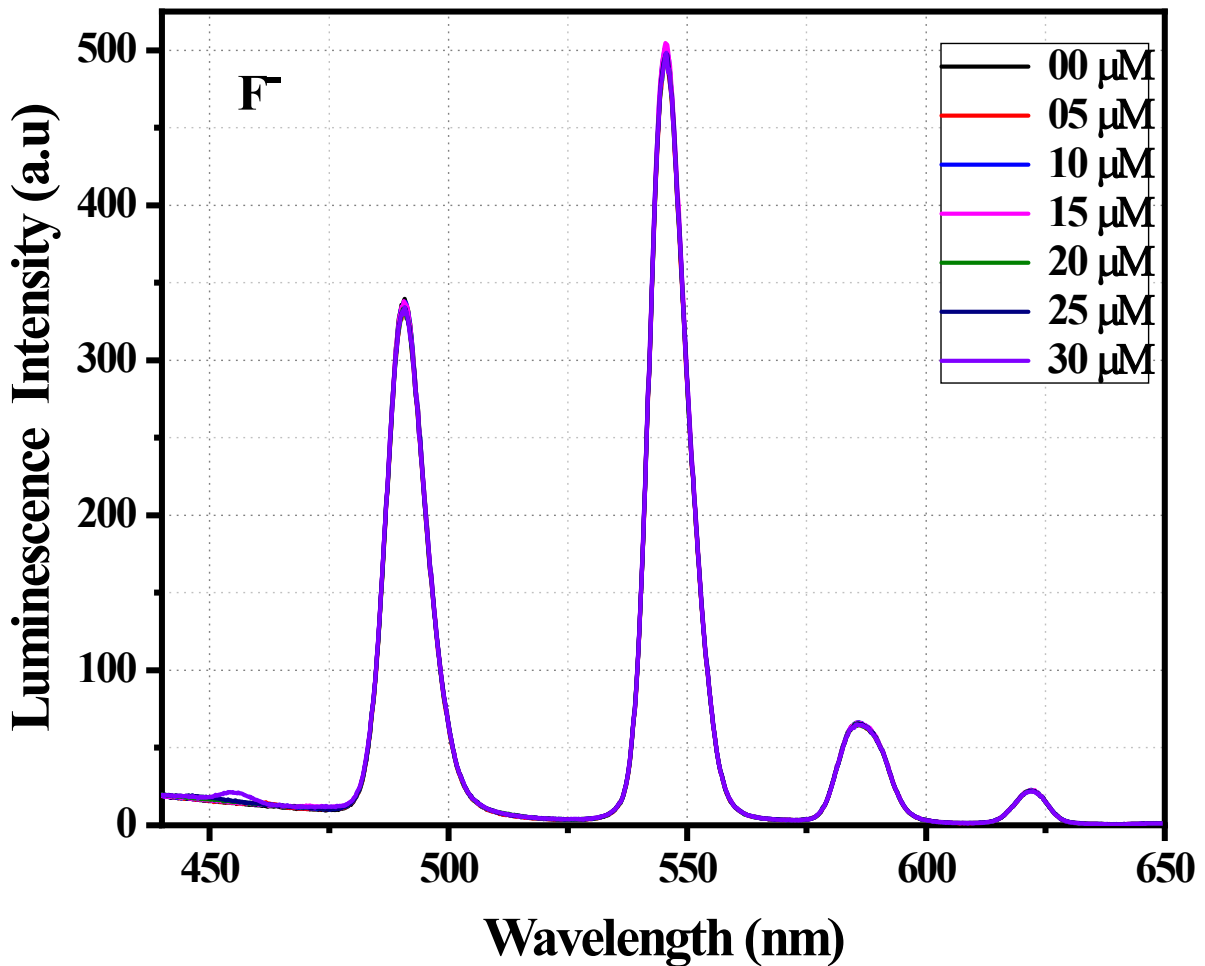


Fig. S9. Emission spectra of **Tb@1** dispersed in water upon the incremental addition of an aqueous solution of F^- ions ($\lambda_{\text{ex}} = 270 \text{ nm}$). The final concentration of F^- ions in the medium is indicated in the legend.

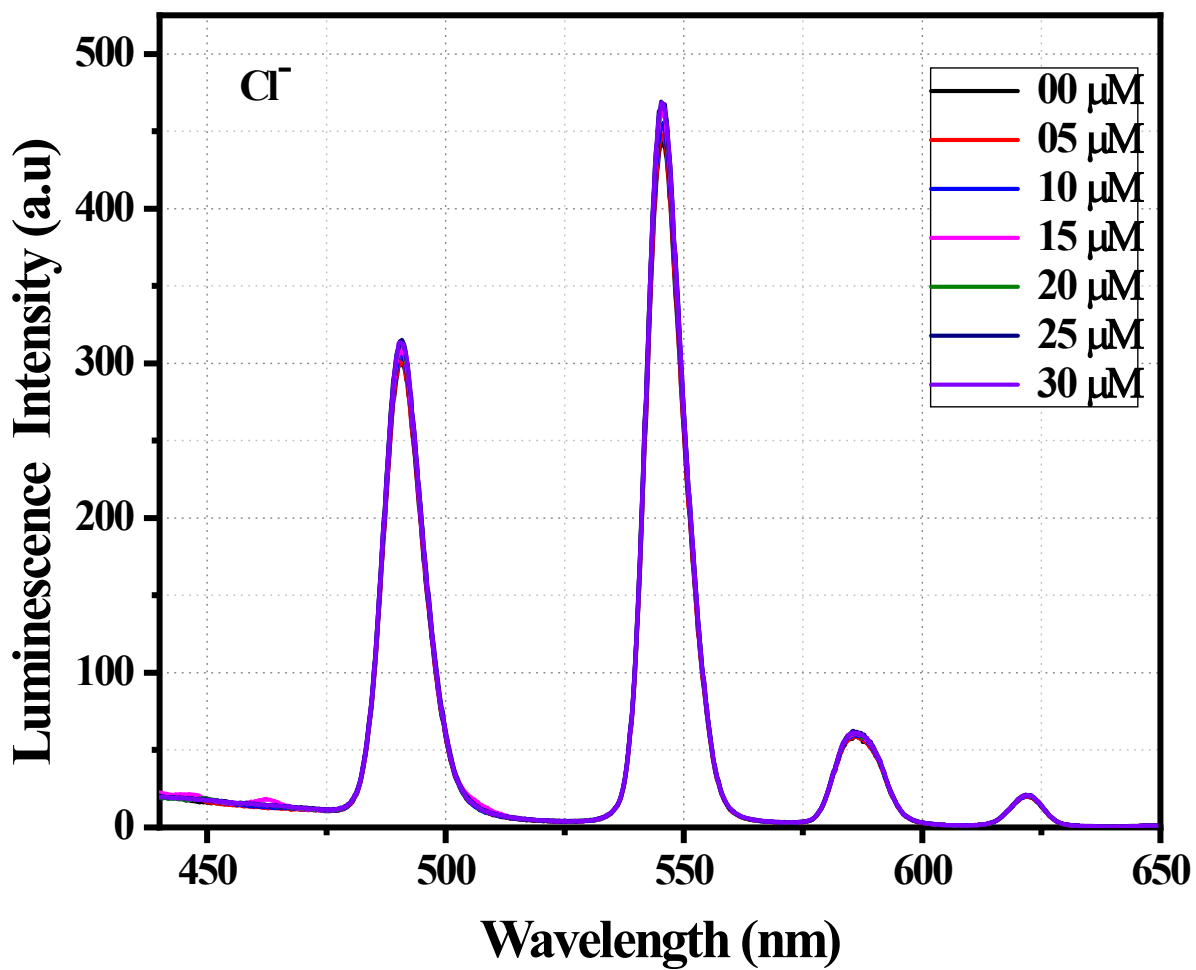


Fig. S10. Emission spectra of **Tb@1** dispersed in water upon the incremental addition of an aqueous solution of Cl⁻ ions ($\lambda_{\text{ex}} = 270 \text{ nm}$). The final concentration of Cl⁻ ions in the medium is indicated in the legend.

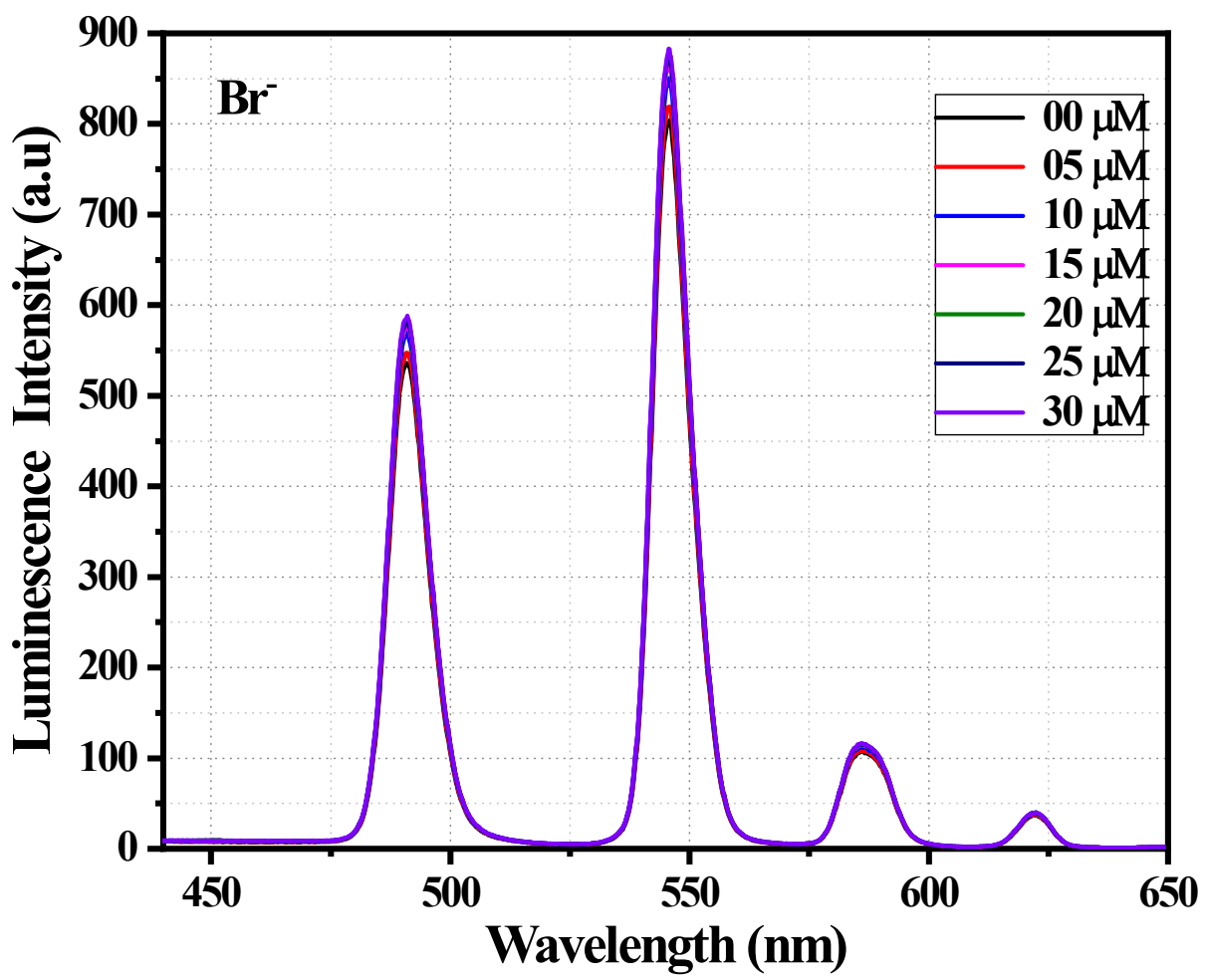


Fig. S11. Emission spectra of **Tb@1** dispersed in water upon the incremental addition of an aqueous solution of Br^- ions ($\lambda_{\text{ex}} = 270$ nm). The final concentration of Br^- ions in the medium is indicated in the legend.

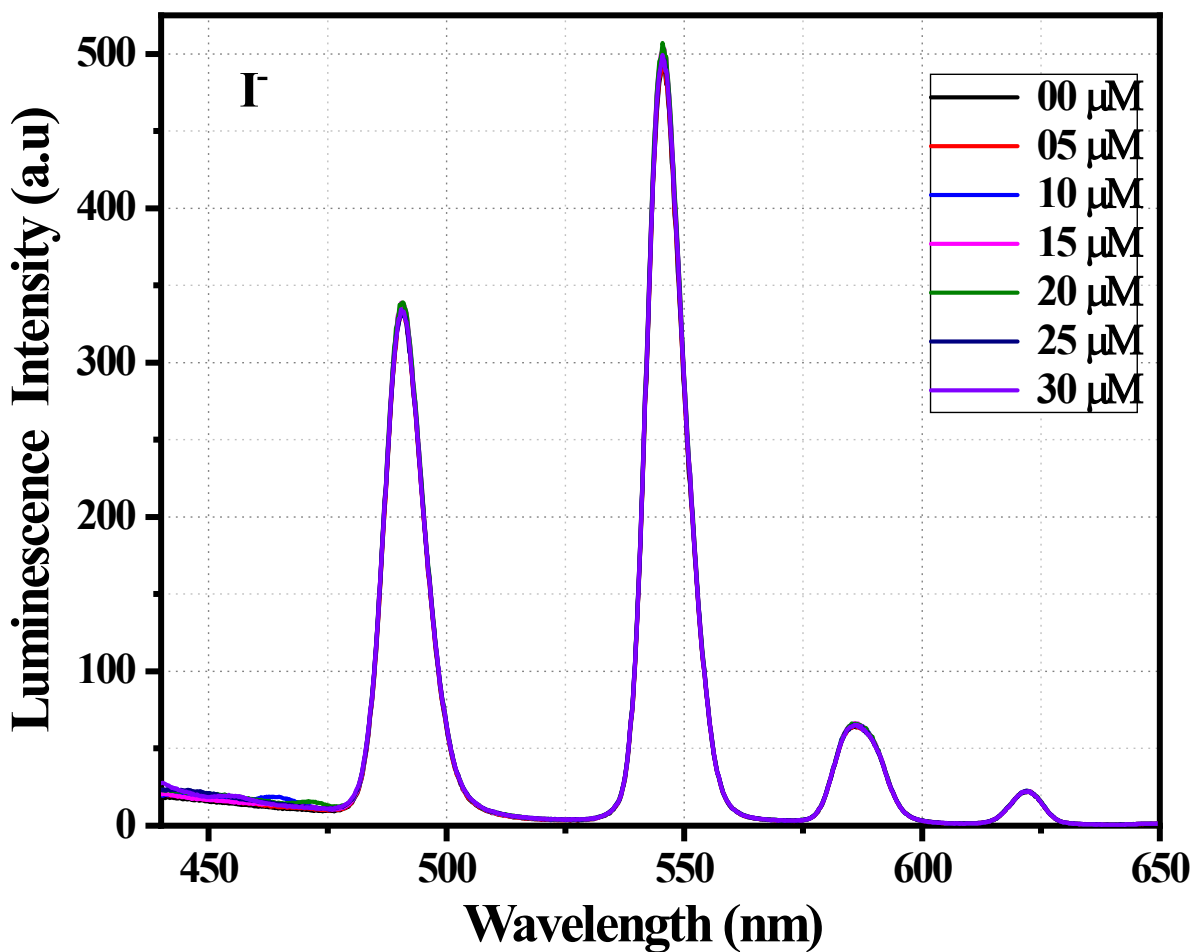


Fig. S12. Emission spectra of **Tb@1** dispersed in water upon the incremental addition of an aqueous solution of I^- ions ($\lambda_{ex} = 270$ nm). The final concentration of I^- ions in the medium is indicated in the legend.

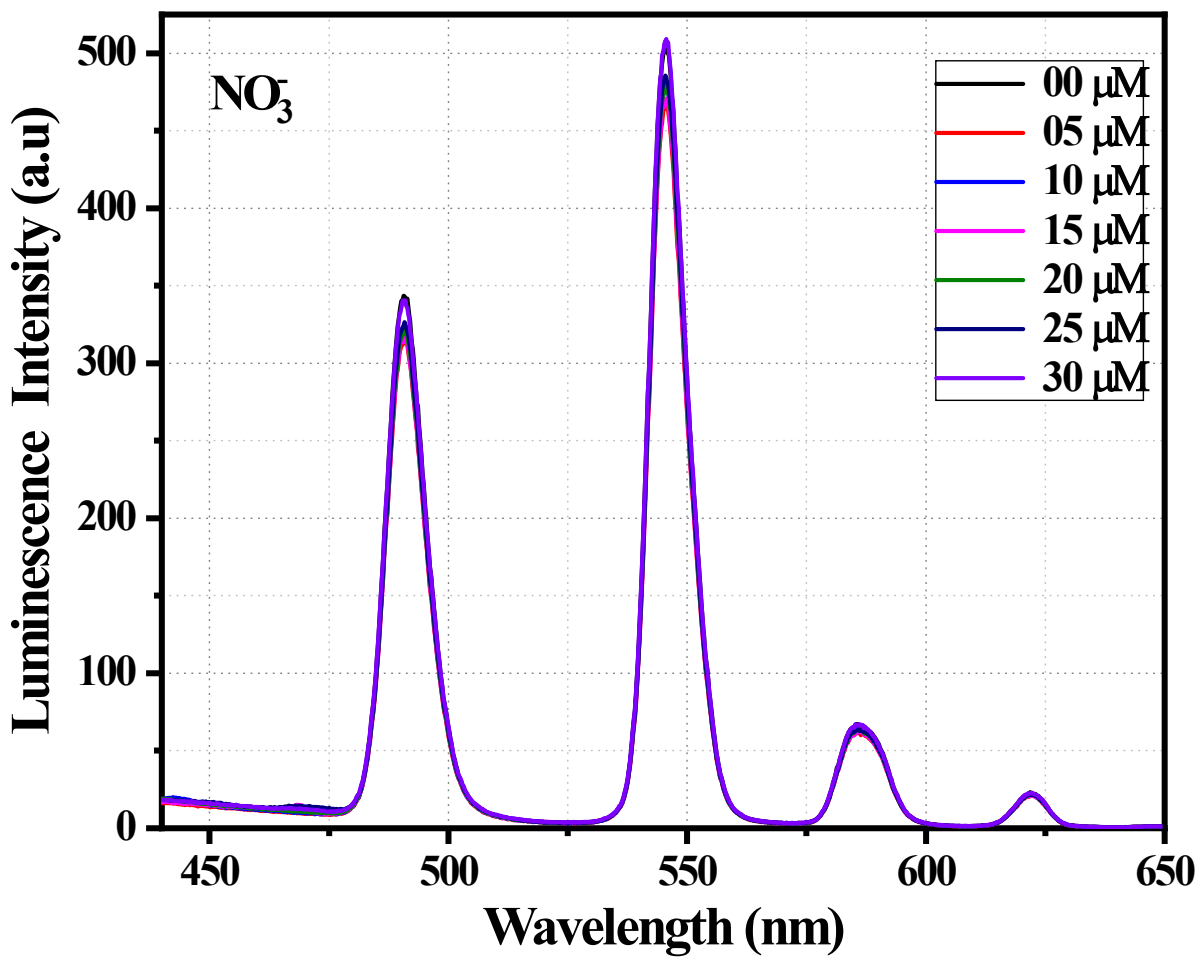


Fig. S13. Emission spectra of **Tb@1** dispersed in water upon the incremental addition of an aqueous solution of NO_3^- ions ($\lambda_{\text{ex}} = 270 \text{ nm}$). The final concentration of NO_3^- ions in the medium is indicated in the legend.

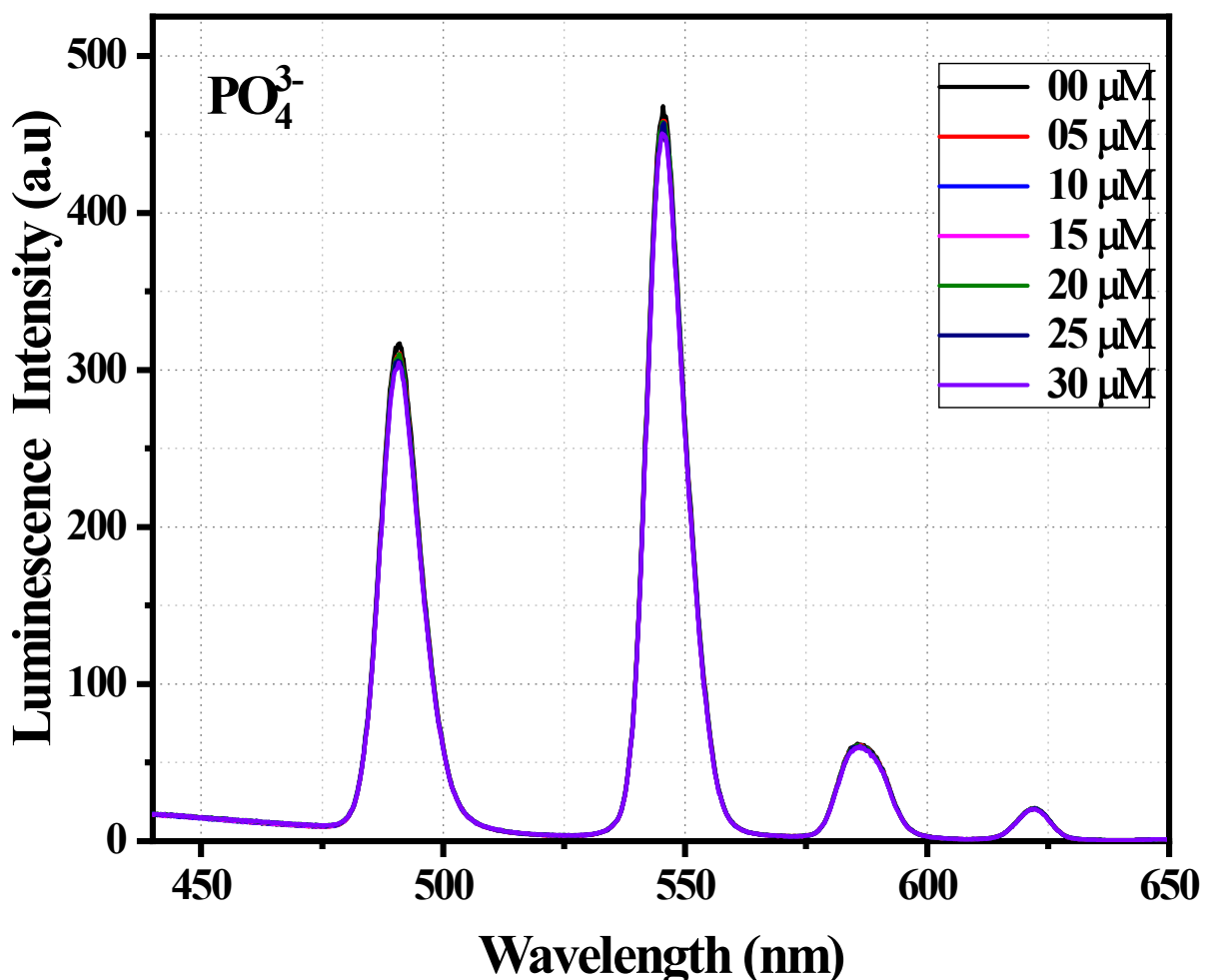


Fig.S14. Emission spectra of **Tb@1** dispersed in water upon the incremental addition of an aqueous solution of PO_4^{3-} -ions ($\lambda_{\text{ex}} = 270 \text{ nm}$). The final concentration of PO_4^{3-} , ions in the medium is indicated in the legend.

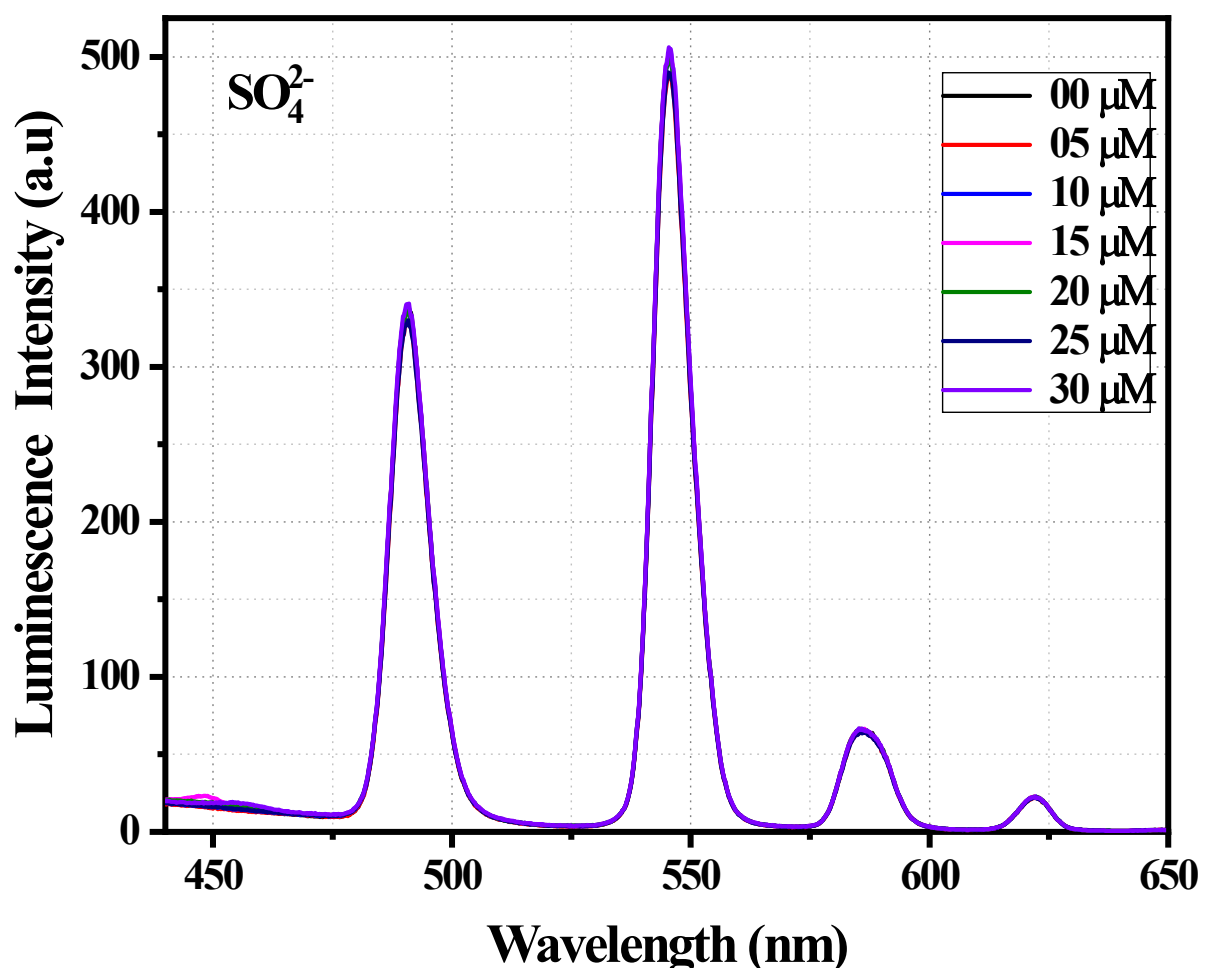


Fig. S15. Emission spectra of **Tb@1** dispersed in water upon the incremental addition of an aqueous solution of SO_4^{2-} -ions ($\lambda_{\text{ex}} = 270 \text{ nm}$). The final concentration of SO_4^{2-} ions in the medium is indicated in the legend.

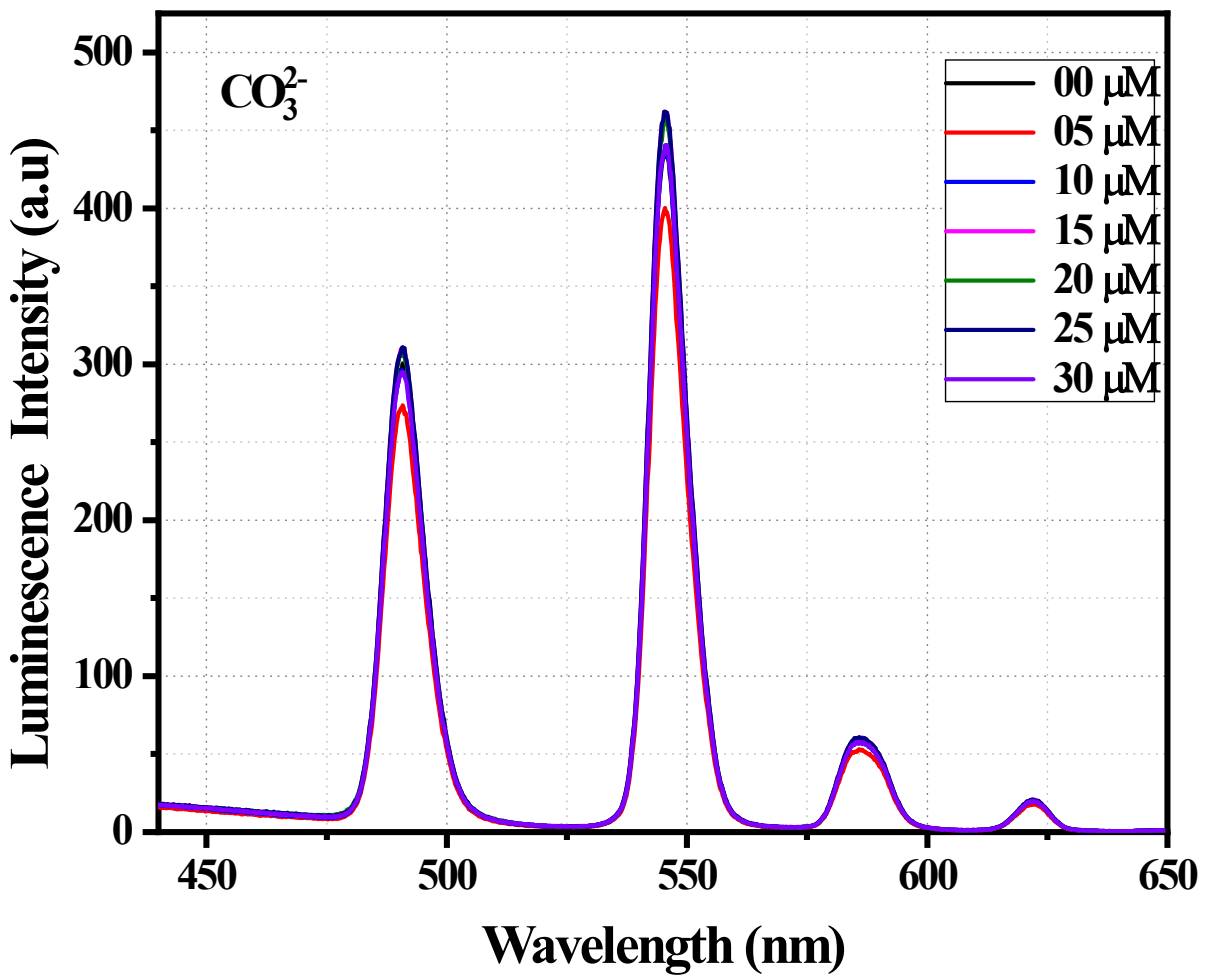


Fig. S16. Emission spectra of **Tb@1** dispersed in water upon the incremental addition of an aqueous solution of CO_3^{2-} -ions ($\lambda_{\text{ex}} = 270$ nm). The final concentration of CO_3^{2-} -ions in the medium is indicated in the legend.

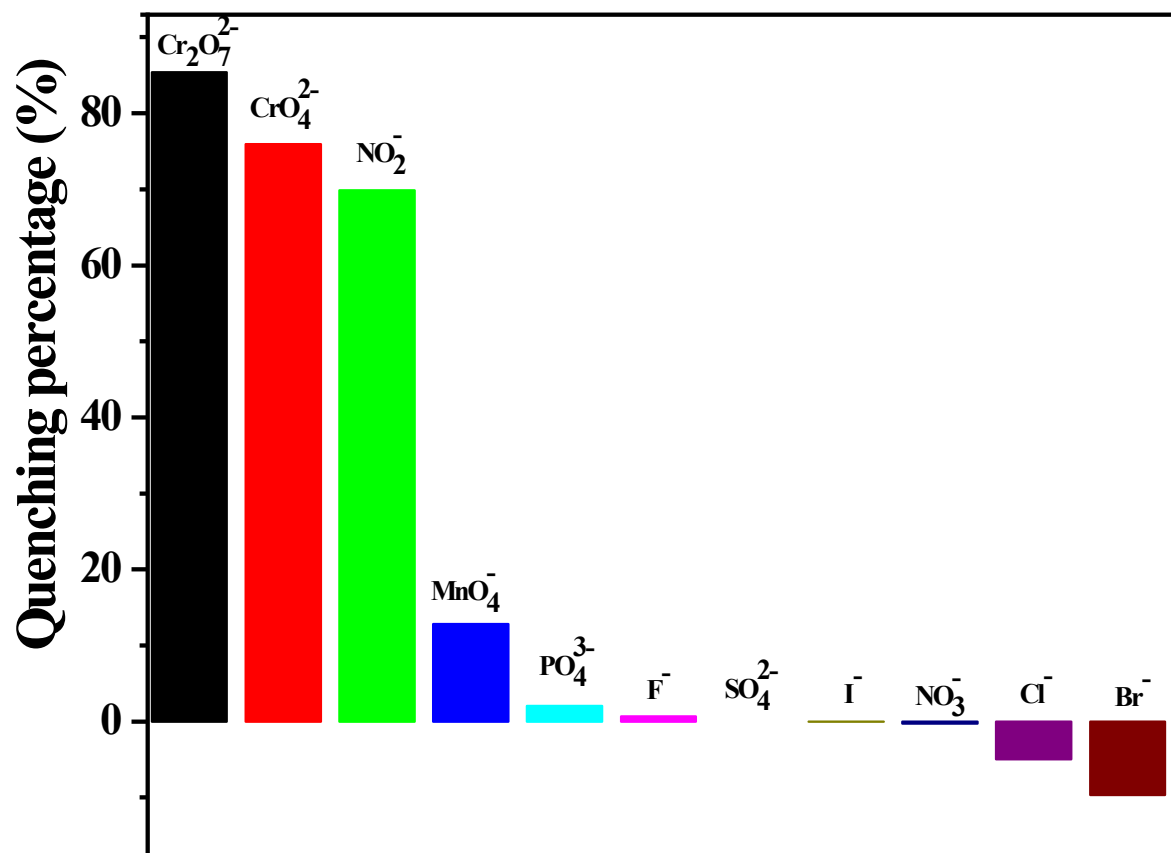


Fig. S17. Quenching efficiency of **Tb@1** toward different anions after the addition of 30 μM of these anions.

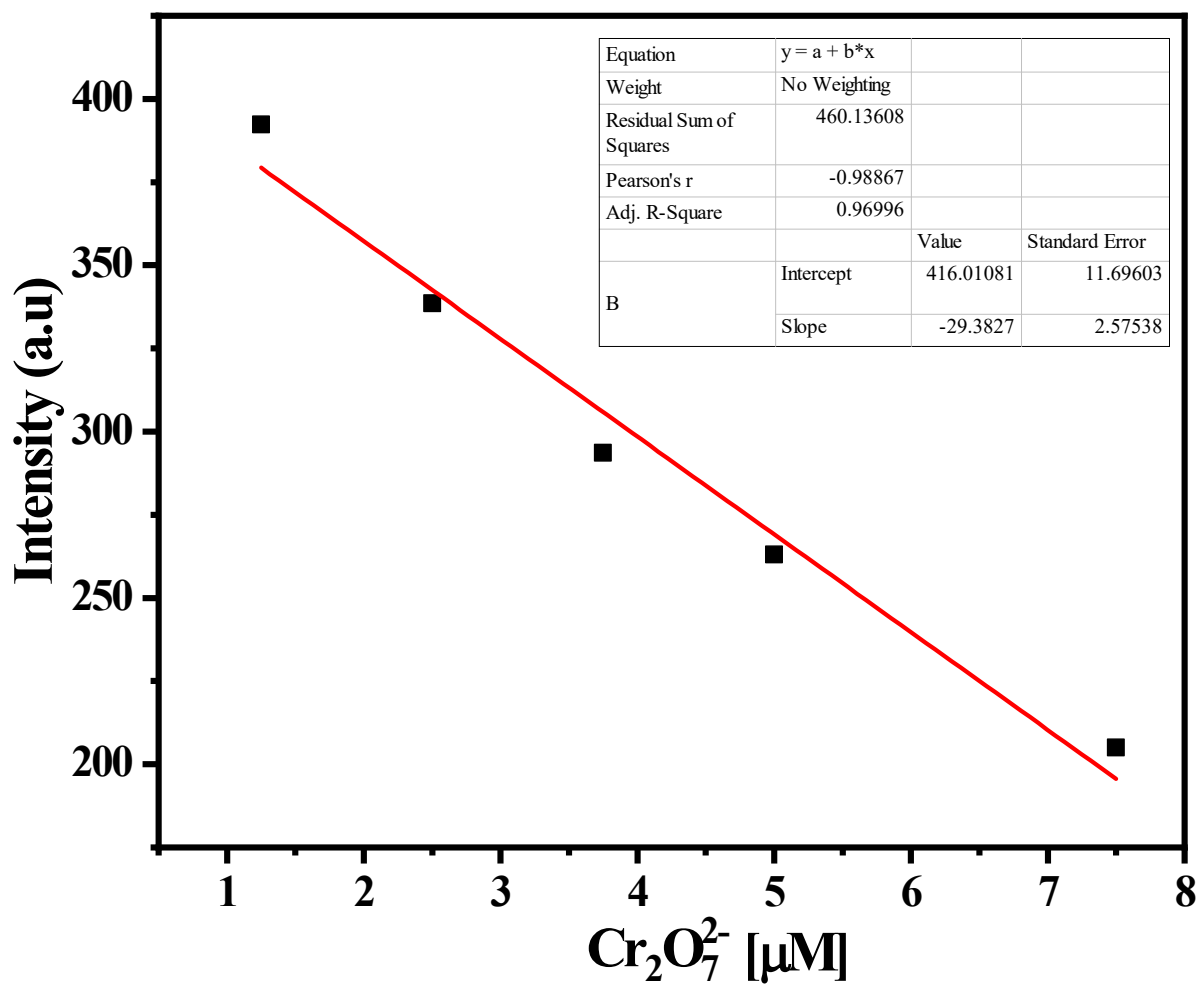


Fig. S18. Linear correlation between the luminescence intensity and concentration of dichromate anion ($\text{Cr}_2\text{O}_7^{2-}$).

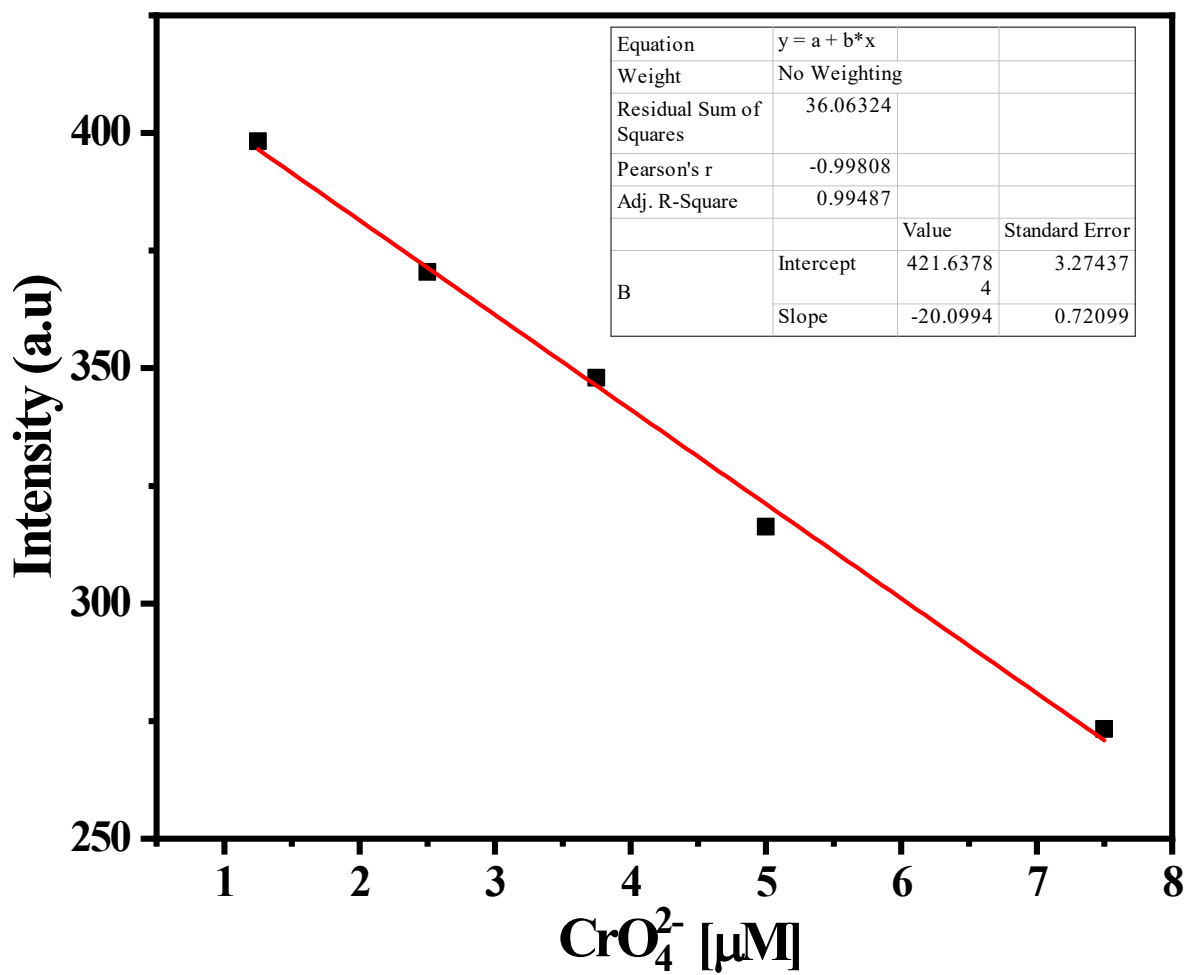


Fig. S19. Linear correlation between the luminescence intensity and concentration of chromate anion (CrO_4^{2-}).

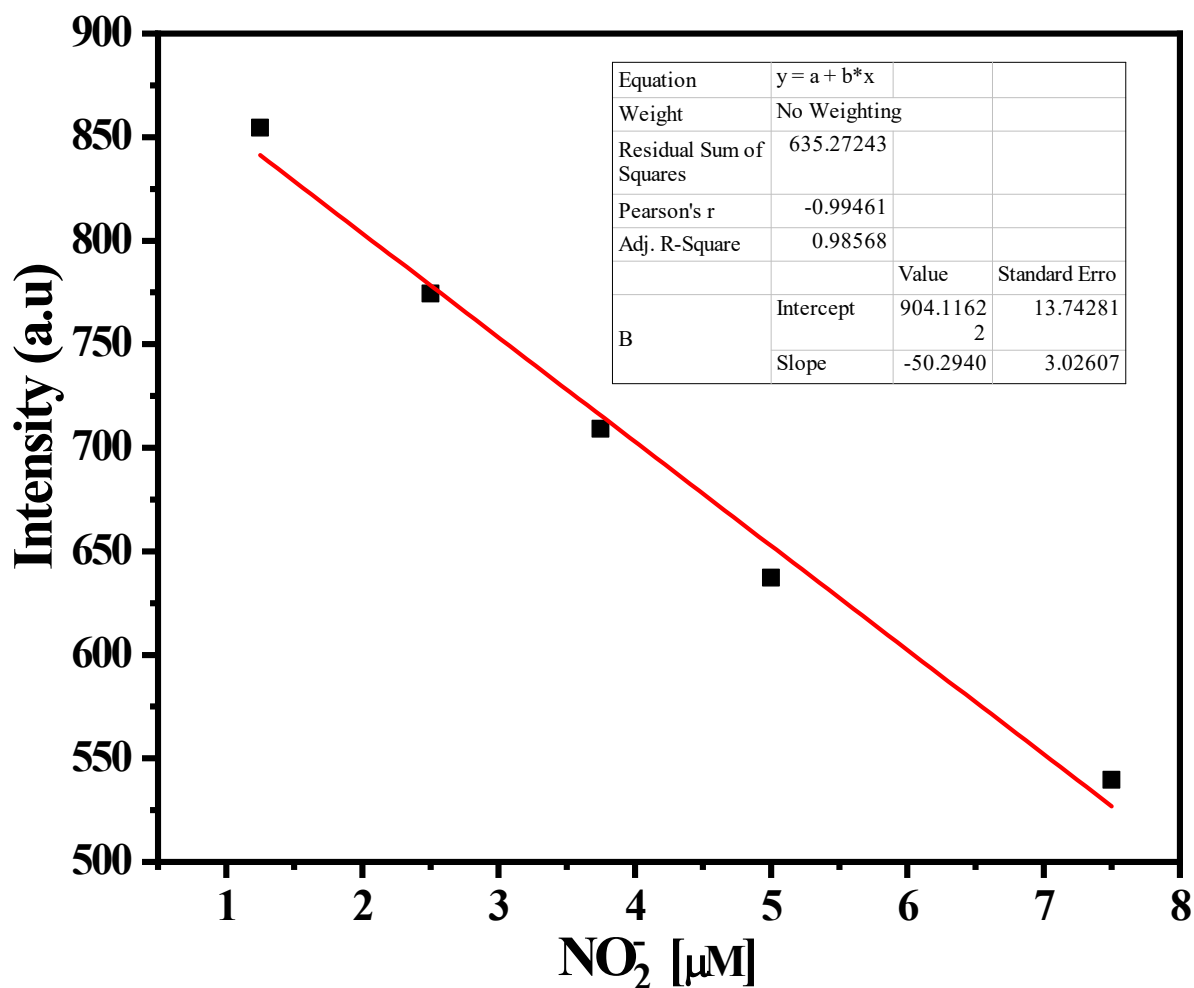


Fig. S20. Linear correlation between the luminescence intensity and concentration of anion (NO_2^-).

The limit of detection (LOD) was calculated by the following equation, $LOD = 3\sigma/m$, where σ denotes the standard deviation of the luminescence intensity (at 546 nm) of 1a without any analytes and m represents the slope of the plot of luminescence intensity data vs concentration of anions.

Table S2: Calculation of standard deviation and Limit of Detection (LOD) for $Cr_2O_7^{2-}$, CrO_4^{2-} and NO_2^- :

Blank Reading (only Composite)	Luminescence intensity at 546 nm (X)	Mean (\bar{x})	Standard Deviation(σ)
Reading 1	788.4	795.6	4.9042
Reading 2	792.6		
Reading 3	795.7		
Reading 4	798.6		
Reading 5	802.7		

Slope, m for $Cr_2O_7^{2-}$ = 29.3827

Slope, m for CrO_4^{2-} = 20.0994

Slope, m for NO_2^- = 50.2940

LOD for $Cr_2O_7^{2-}$ = $3\sigma/m = (3 \times 4.9042)/29.3827=0.5007 \mu M=147.306 ppb$

LOD for CrO_4^{2-} = $3\sigma/m = (3 \times 4.9042)/20.0994=0.7319 \mu M=142.150 ppb$

LOD for NO_2^- = $3\sigma/m = (3 \times 4.9042)/50.2940=0.2925 \mu M= 20.183 ppb$

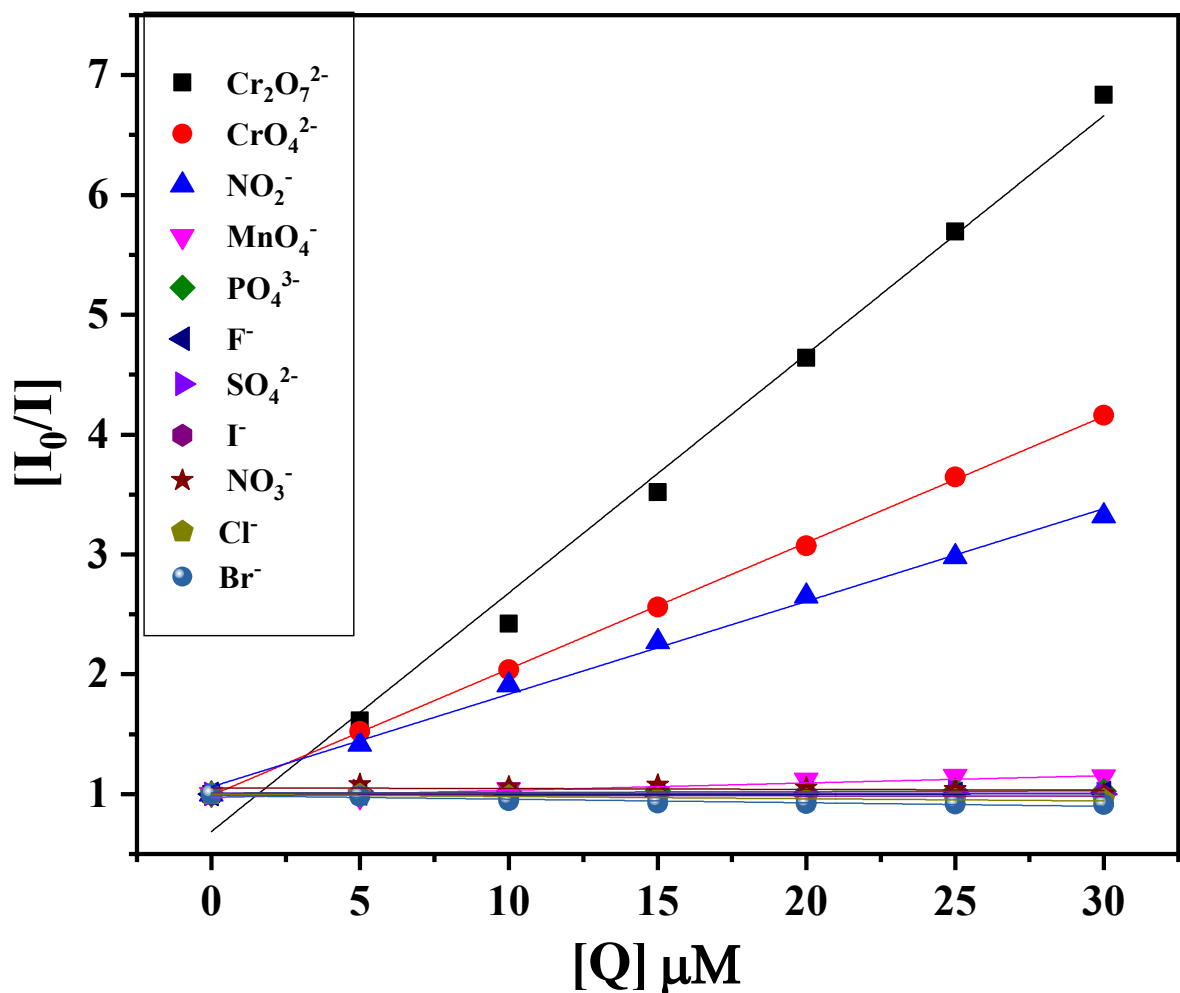


Fig. S21. K_{SV} curves of **Tb@1** in an aqueous solution in the presence of all the studied anions.

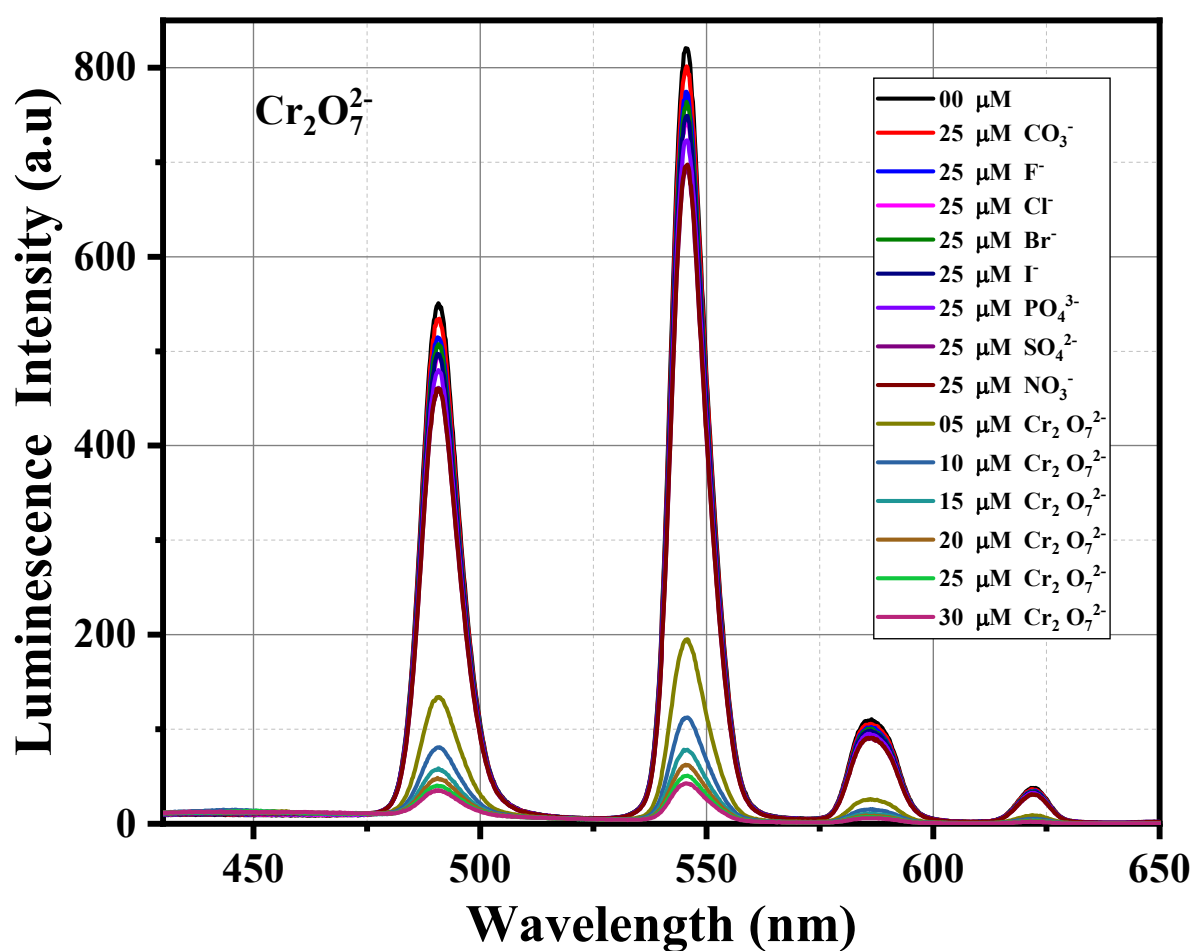


Fig. S22a. Emission spectra of **Tb@1** in water dispersion upon the incremental addition of Cr₂O₇²⁻ solution in the presence of 25 μM of different anion solution ($\lambda_{\text{ex}} = 270 \text{ nm}$).

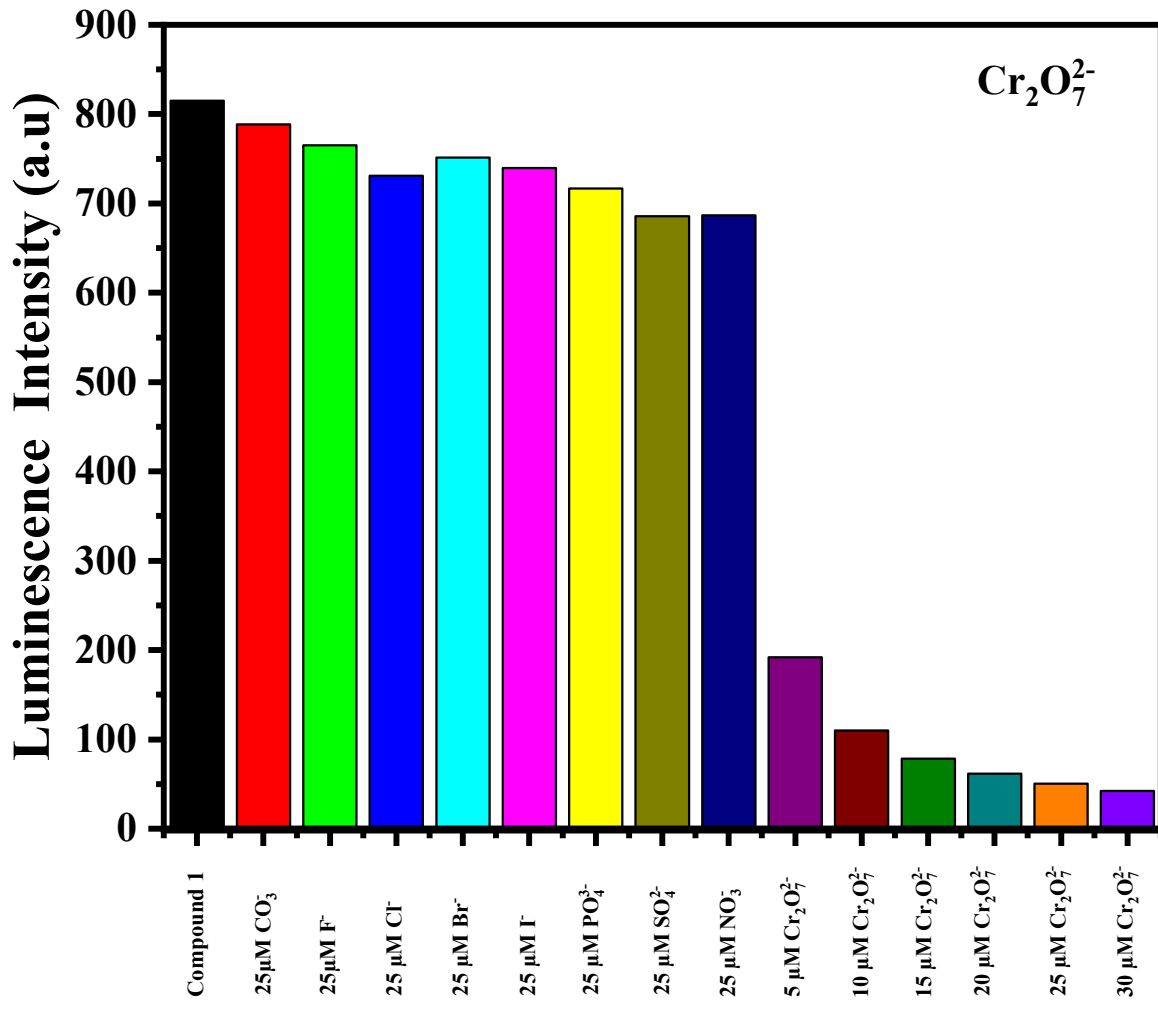


Fig. S22b. Corresponding bar diagram showing the luminescence intensity (monitored at 545 nm) after the sequential addition of the analytes.

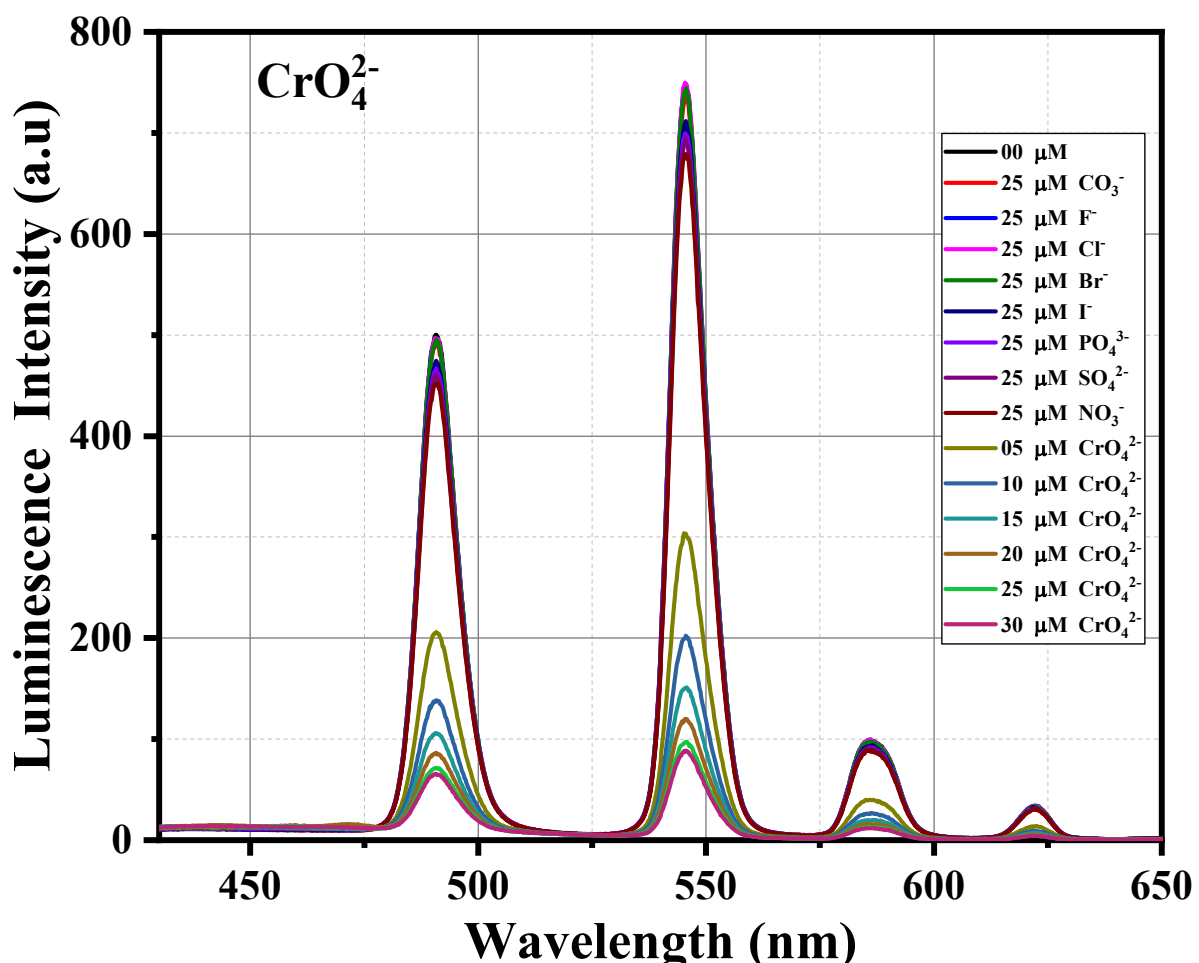


Fig. S23a. Emission spectra of composite in water dispersion upon the incremental addition of CrO_4^{2-} solution in the presence of 25 μM of different anion solution ($\lambda_{\text{ex}} = 270 \text{ nm}$).

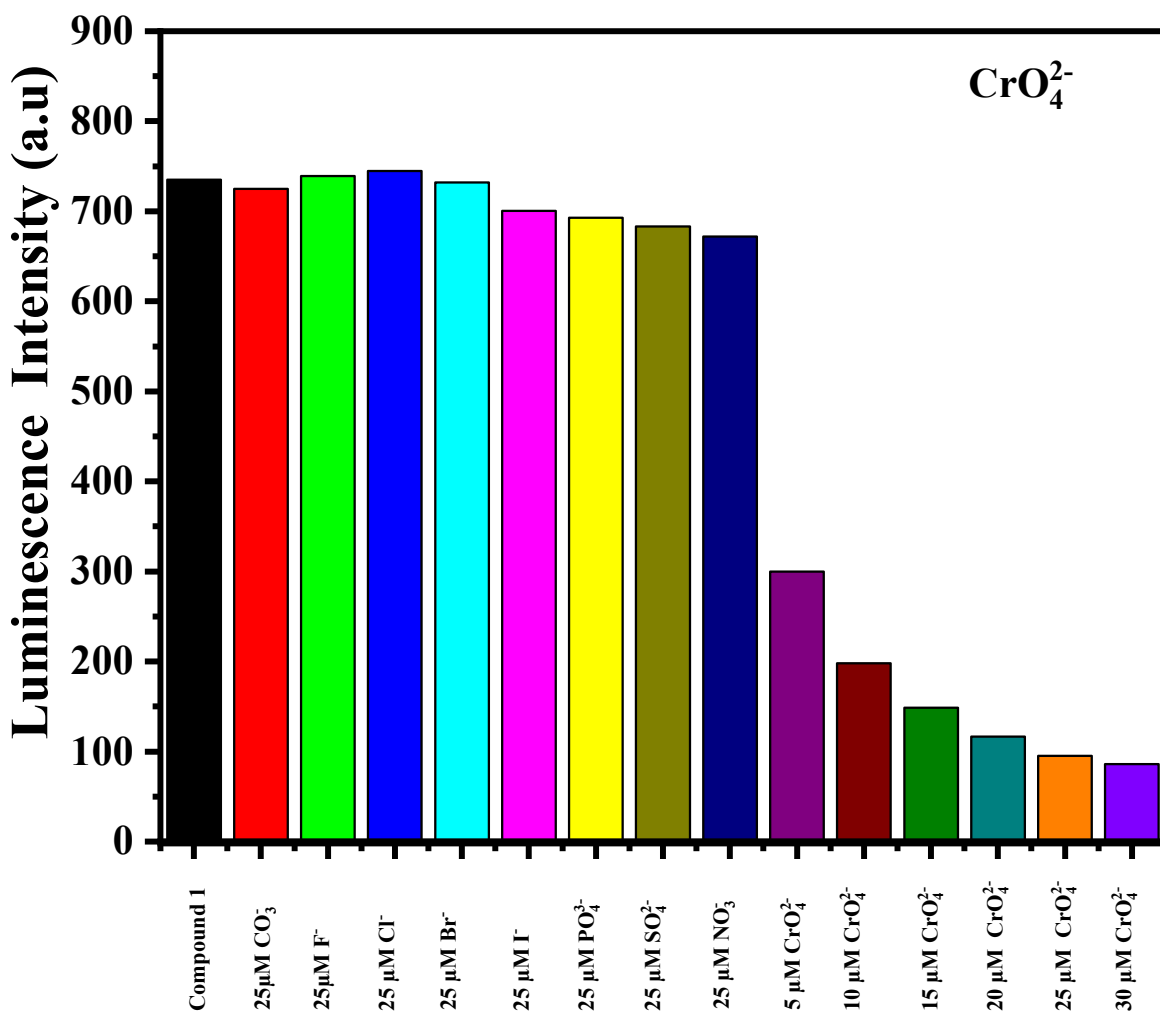


Fig. S23b. Corresponding bar diagram showing the luminescence intensity (monitored at 545 nm) after the sequential addition of the analytes.

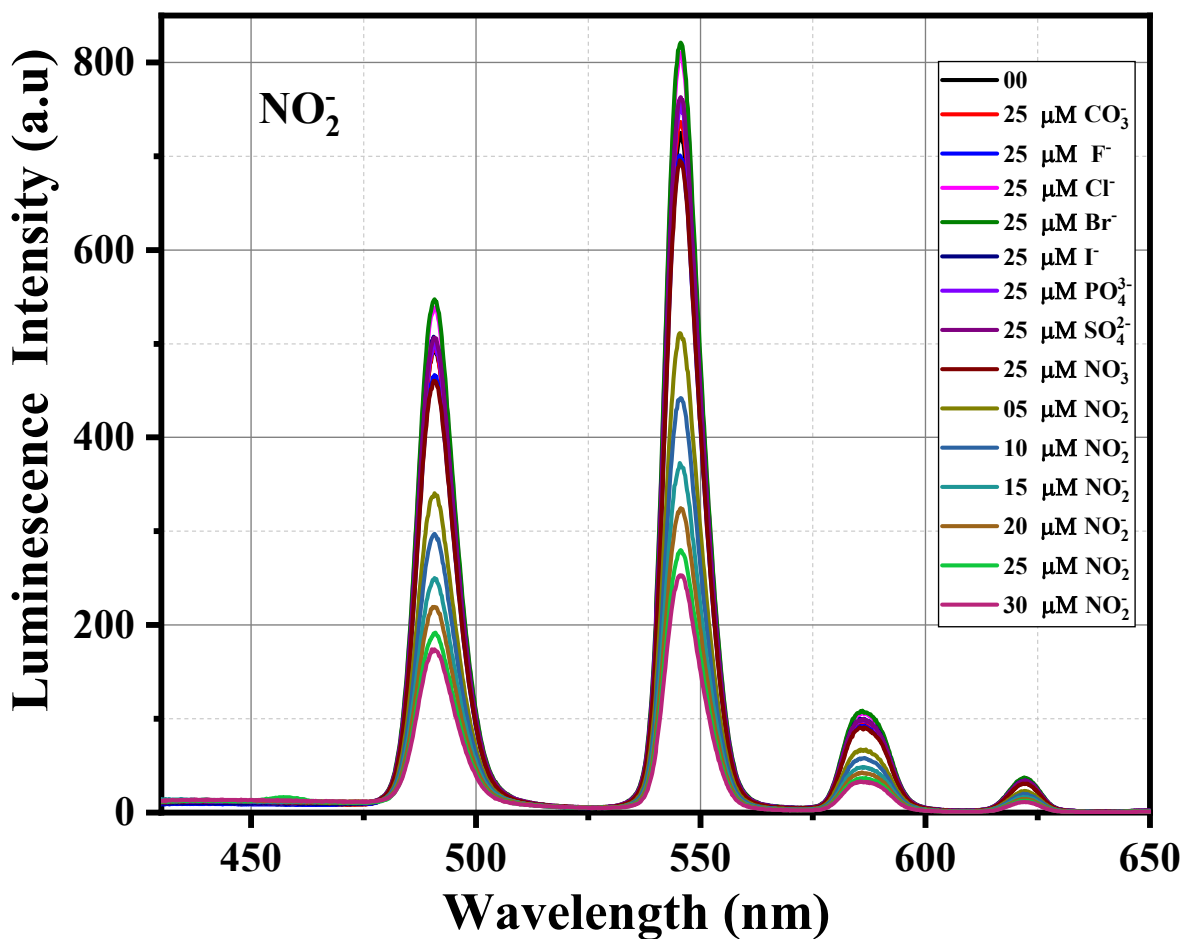


Fig. S24a. Emission spectra of composite in water dispersion upon the incremental addition of NO_2^- solution in the presence of 25 μM of different anion solution ($\lambda_{\text{ex}} = 270 \text{ nm}$).

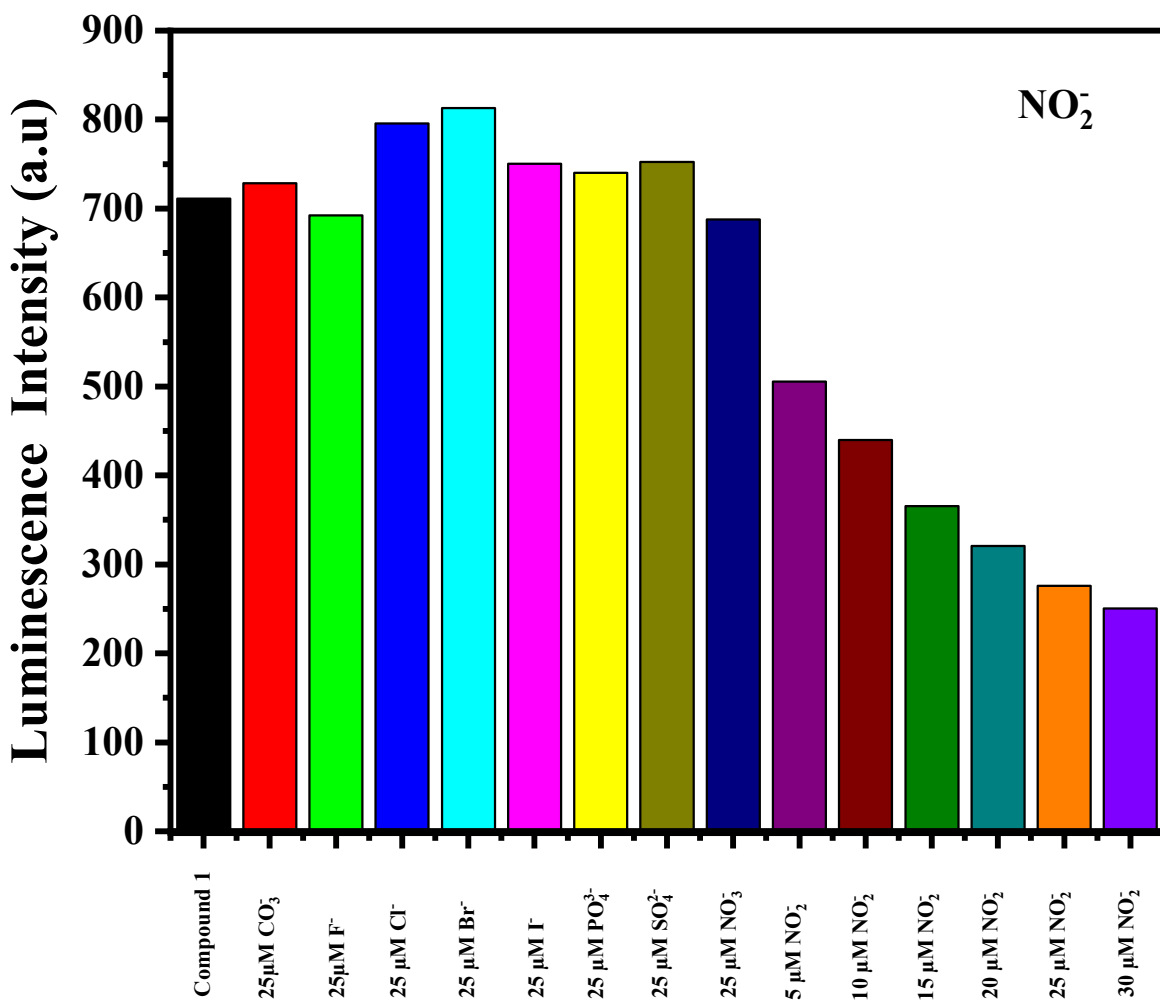


Fig. S24b. Corresponding bar diagram showing the luminescence intensity (monitored at 545nm) after the sequential addition of the analytes.

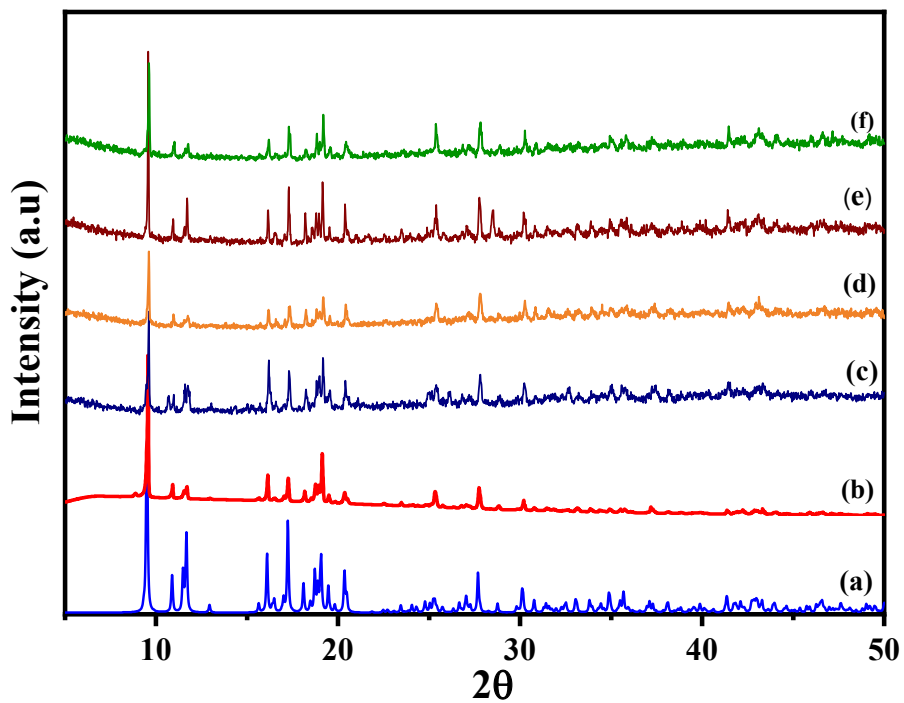


Fig. S25. The PXRD pattern of (a) Simulated of compound **1**, (b) Experimental of compound **1**, (c) compound **1** immersed in aqueous solution of $\text{Tb}(\text{NO}_3)_3$ (composite **Tb@1**), (d) composite **Tb@1** immersed in an aqueous solution of $\text{Cr}_2\text{O}_7^{2-}$, (e) composite **Tb@1** immersed in an aqueous solution of CrO_4^{2-} , (f) composite **Tb@1** immersed in an aqueous solution of NO_2^- .

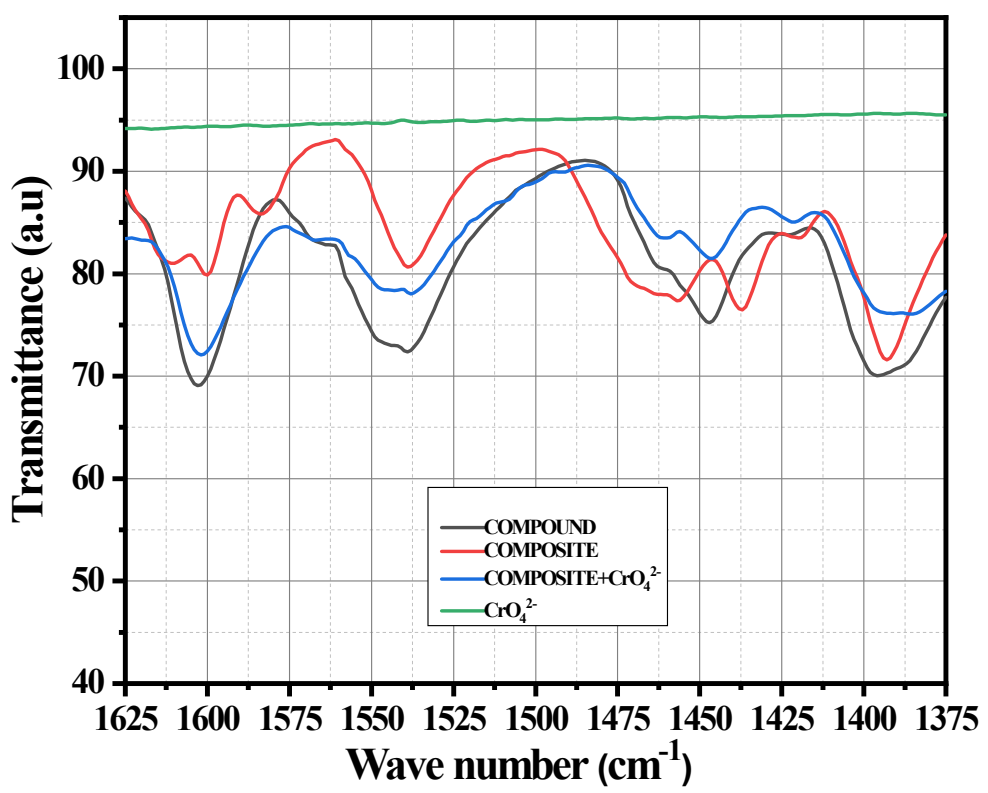


Fig. S26. FTIR spectra of compound **1**, composite (**Tb@1**), composite (**Tb@1**) + K₂CrO₄ and pure K₂CrO₄ in the range 1625 to 1375 cm⁻¹.

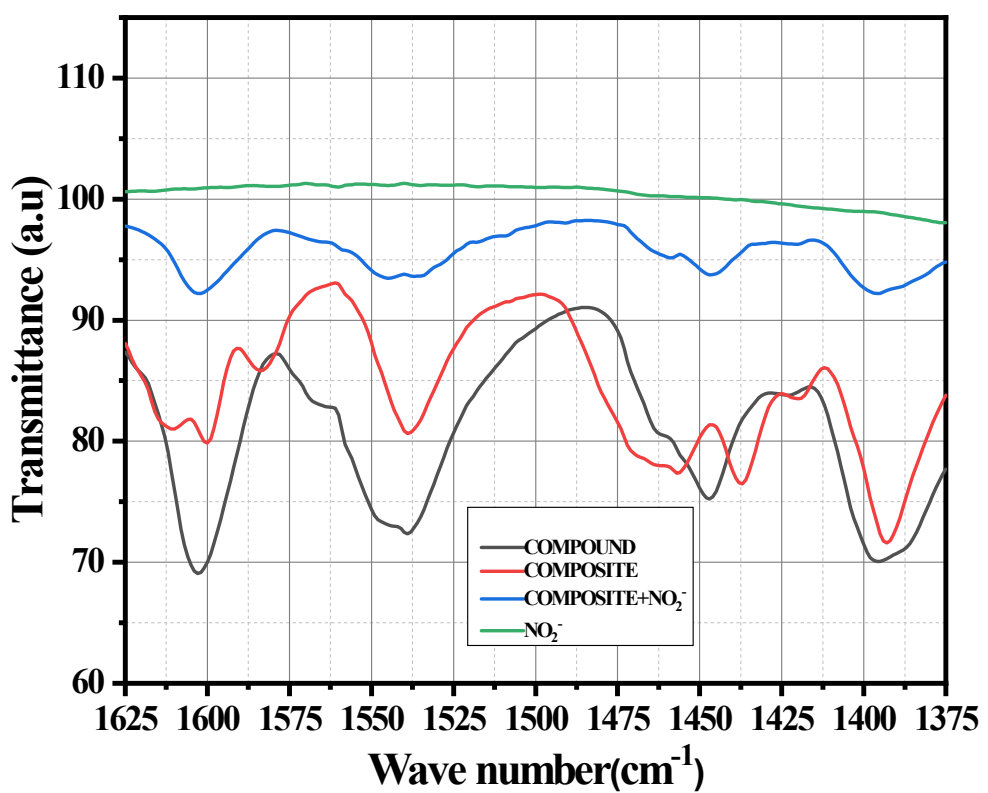


Fig. S27. FTIR spectra of compound **1**, composite (**Tb@1**), composite (**Tb@1**) + NaNO₂ and pure NaNO₂ in the range 1625 to 1375 cm⁻¹.